European Nb_3Sn and Nb–Ti strand verification for ITER: processing, measurements and statistical analysis

M J Raine[1], T Boutboul[2,‡], P Readman[2] and D P Hampshire[1]

[1]Durham Fusion Energy Reference Laboratory, Superconductivity Group, Centre for Materials Physics, Department of Physics, Durham University, South Road, Durham, DH1 3LE, UK

[2]ITER Delivery Department, Fusion for Energy, 08019 Barcelona, Spain‡

E-mail: m.j.raine@durham.ac.uk

Abstract.

We present a large quantity ($\sim 13\,000$) of verification measurements (critical current (I_c), n-value, hysteresis loss (Q), residual resistivity ratio (RRR), twist-pitch, diameter, plating thickness and copper-non-copper ratio) and statistical analysis of internal tin and bronze route Nb_3Sn and Nb-Ti strands used in the ITER tokamak magnet system. The Durham laboratory partnered the relevant manufacturer and each independently processed-and-measured one of two short adjacent strands taken from the ends of thousands of piece-lengths, typically several kilometres long. Processing included heat-treatment of the Nb_3Sn, which is an irreversible process (i.e. destructive of as-supplied strands).

Here we show that when repeat processing-and-measurement of the same piece of Nb_3Sn strand is not possible, although the similarity between adjacent strands is not known *a priori*, processing-and-measuring adjacent strands provides a proxy for single lab (with repeat) measurements or round-robin measurements (i.e. without processing). Processing-and-measuring adjacent strands provides limits for the errors introduced by laboratories and for the variability of the piece-lengths, rather than the specific values that round-robin measurements provide. This is because it is not possible to distinguish whether unidentified sources of error come from the differences between adjacent strands or from unidentified laboratory errors, such as from gas impurities during heat-treatment or strand handling.

We categorise different types of processing-and-measurement: one type includes I_c of bronze route Nb_3Sn where the maximum lab errors are similar to the well-known estimated lab errors that are found using, for example, the commercially specified accuracy of the instruments. Furthermore, the possibility of unidentified sources of random lab error is excluded, and both piece-length variability and lab errors are specified - similar to round-robin measurements. In another type (e.g. RRR or Q of internal tin Nb_3Sn), larger than expected variances are measured and unidentified sources of error operate. Categorising the different types of processing-and-measurement helps identify routes for improvement.

Keywords: ITER, Magnets, Superconductors, Verification, Strand, Nb_3Sn, Nb-Ti,

‡ Current address: CERN, Magnets, Superconductors and Cryostats Group, 1211 Geneva 23.

1 Introduction

The development of standardised measurements has been an integral part of the progress of international science and commerce. However, choosing the best metrology for measuring industrial materials is complex because one needs to optimise cost, accuracy and resilience, which change depending on the quantity and properties of the materials being measured, as well as the local environment. In the current (pre-commercial) phase of large-scale commercial fusion programs, several competing organisations will require reliable, large quantity measurements to be made by independent laboratories that also protect conductor manufacturer know-how and commercial interests. Some university groups are ideal candidates to take up such roles. Here we present results of thousands of verification measurements made by strand manufacturers and Durham on pairs of adjacent Nb_3Sn strands ~ 25 m in length, and adjacent Nb-Ti strands ~ 5 m in length, that were cut from the ends of piece-lengths several km long. They were fabricated as part of the European Union's (EU) contribution to the ITER tokamak magnet system.

In Durham, over 5500 strands were received, $\sim 13\,000$ measurements made, and 21 reports delivered. While Durham began with the necessary expertise and experience to make such measurements on small strand quantities [1], the combined size of the contracts received, coupled with a need to meet delivery deadlines, required a rapid and substantial up-scaling in equipment, personnel, training, strand and data handling, and measurement methodologies. This work was subsequently extended to include measurements of the critical current (I_c) on ~ 1400 Nb_3Sn witness samples, as well as measurements on Nb-Ti strands intended for use in Poloidal Field (PF) Coil 6 [2] - followed by a down-scaling back to original capacity.

Here, we outline our approach to our statistical analysis, by first comparing it with a single lab that's (only) measuring (i.e. not processing) the critical currents of a collection of superconducting strands, or more specifically, piece-length ends. The variance of the data ($\sigma^2_{Lab\,1\,data}$) from the lab includes a contribution from both the strand variability ($\sigma_{Strand\,variability}$) as well as the broadening from the random lab errors ($\sigma_{Lab\,1\,errors}$) introduced during the measurements where,

$$\sigma^2_{Lab\,1\,data} = \sigma^2_{Strand\,variability} + \sigma^2_{Lab\,1\,errors}\,. \tag{1}$$

In principle, one can estimate the random lab errors (for example from the commercially specified inaccuracies of the instruments) and use Eq. 1 to find a value for the variability of the strands. This approach, however, is limited by not knowing whether or not there are unidentified sources of random lab error and is therefore, strictly, a lower bound. Fortunately, these uncertainties can be eliminated by making repeat measurements on one of the strands from the piece-length ends. The variance of these repeat data ($\sigma^2_{Lab\,1\,R.data}$) is only dependent on the random lab errors where,

$$\sigma^2_{Lab\,1\,R.data} = \sigma^2_{Lab\,1\,errors}\,, \tag{2}$$

and Eqs. 1 and 2 together provide measured values for both the lab errors and the variability of the strands. If the measured value of $\sigma_{Lab\,1\,errors}$ is the same as the estimated random lab errors, one can conclude that all the important sources of random error in the measurements have been identified. If not, there are additional unidentified sources of random lab error in the measurements. We also note that the information repeat measurements bring, need not necessarily be obtained by the same lab, but is also available in round-robin experiments. Even if we have just two labs measuring the same collection of superconducting strands, we have for the second lab,

$$\sigma^2_{Lab\,2\,data} = \sigma^2_{Strand\,variability} + \sigma^2_{Lab\,2\,errors}\,. \tag{3}$$

The round-robin must be 'ideal' in the sense that we assume no progressive damage or changes in the strands due to, for instance, transport between the labs or strand handling. In this case, the equation equivalent to Eq. 2 for the repeat measurements, obtained from the sum of variances law, is

$$\sigma^2_{\Delta} = \sigma^2_{Lab\,1\,errors} + \sigma^2_{Lab\,2\,errors}\,, \tag{4}$$

where σ^2_{Δ} is the variance of the difference between the pairs of, say, I_c measurements in the two labs on the same strands from the piece-length ends. Solving the three equations 1, 3 and 4 again gives specific measured values for the three unknowns, the strand variability and the two lab errors, without the need for estimates.

In this work, the processing-and-measurement at cryogenic temperatures of each adjacent Nb_3Sn strand necessarily includes an irreversible heat-treatment, independently performed by each lab on their specific strand. These heat-treatments introduce additional variation in the measured properties. Since each heat-treatment cannot be repeated, repeat processing-and-measurement on the same piece of strand or round-robin processing-and-measurement cannot be used. Despite this, and the complexity that it is unknown *a priori* whether adjacent strands have similar properties, here we extract the information analogous to that from repeat measurements from the correlation in the data from the adjacent strands. We demonstrate that in general, measuring-and-procesing adjacent strands give limits for the lab errors and the strand variabilities, rather than the specific values found from round-robin measurements. Nevertheless, for some types of processing-and-measurement, the adjacent strands are identical, the upper and lower bound limits are the same, and as with round-robin measurements, specific values of the random errors introduced by the participating laboratories and the variability associated with the manufacture of the strands can be specified/measured.

The next section describes the context for processing-and-measuring this large quantity of strands. Sections 3 - 6 outline the experimental approach used to do the processing and make the measurements in Durham. Sections 7 and 8 provide the statistical framework, the large datasets and their analysis. In sections 9 and 10 we discuss the different types of processing-and-measurement: those where the lab errors

Table 1: ITER Organisation Domestic Agencies and their Reference Laboratories [6, 7]

Domestic Agency	Reference Laboratory
ITER Organisation	CERN [8]
EU (European Union)	Durham University Superconductivity Group (DUSG) [9]
USA (United States of America)	National High Magnetic Field Laboratory (NHMFL) [10]
China	Insitute of Plasma Physics, Chinese Academy of Sciences (ASIPP) [11, 12]
Japan	Japan Atomic Energy Agency (JAEA) [13]
Korea	Korea Institute of Fusion Energy (KFE) (formerly NFRI) [14]
Russia	Bochvar Research Institute of Inorganic Materials (VNIM) [15, 16]

and strand variablity are well characterised with uncertainties that are accurately known, together with those where the sources of error and variability are unknown. The paper concludes with some final comments and recommendations.

2 The European Union's verification strand and witness sample process.

Prior to the commencement of ITER construction, worldwide production of Nb_3Sn strand was around 15 tonnes per year [3]. By 2012, ITER TF strand production alone had risen to over 120 tonnes per year [4]. The European Union's contribution [5] to the poloidal field coils used 45 tonnes of Nb-Ti to produce $\sim 1/3$ of PF6 (Figure 1). Six of the seven worldwide domestic agencies (DA) responsible to the ITER Organisation (IO) for superconducting strand, of which Fusion for Energy (F4E) was one, had their own qualified reference laboratory (RL) [6]. In addition, IO had its own reference laboratory (CERN) for periodic cross-checks, superconducting materials investigations, trials and training. The worldwide DA's and RL's are listed in Table 1.

2.1 Internal tin (IT) and bronze route (BR) Nb_3Sn strands - TF coils

Initially, 100 % of both the internal tin (IT) and bronze route (BR) Nb_3Sn adjacent strands from the ends of piece-lengths were selected for processing-and-measurement (Table 2), reducing to 50 % and then 25 % in accordance with the ITER Organisation procurement agreement. If the Durham results did not agree with the manufacturer's, further testing at Durham and/or another laboratory (e.g. CERN) was conducted. We note that there were several cross-checks made at CERN, and throughout all campaigns, no significantly different results to those obtained at Durham were found.

2.2 Nb-Ti strands for PF coil 6

The verification processing-and-measurement for the Nb-Ti strands was similar to that of the Nb_3Sn strands (Table 2), but there was no heat-treatment and an additional nickel-plating adhesion measurement (not reported here) was included. Durham received, in one deliverable, 323 lots of 5 m long Nb-Ti strands and completed 2571 measurements (Table 3).

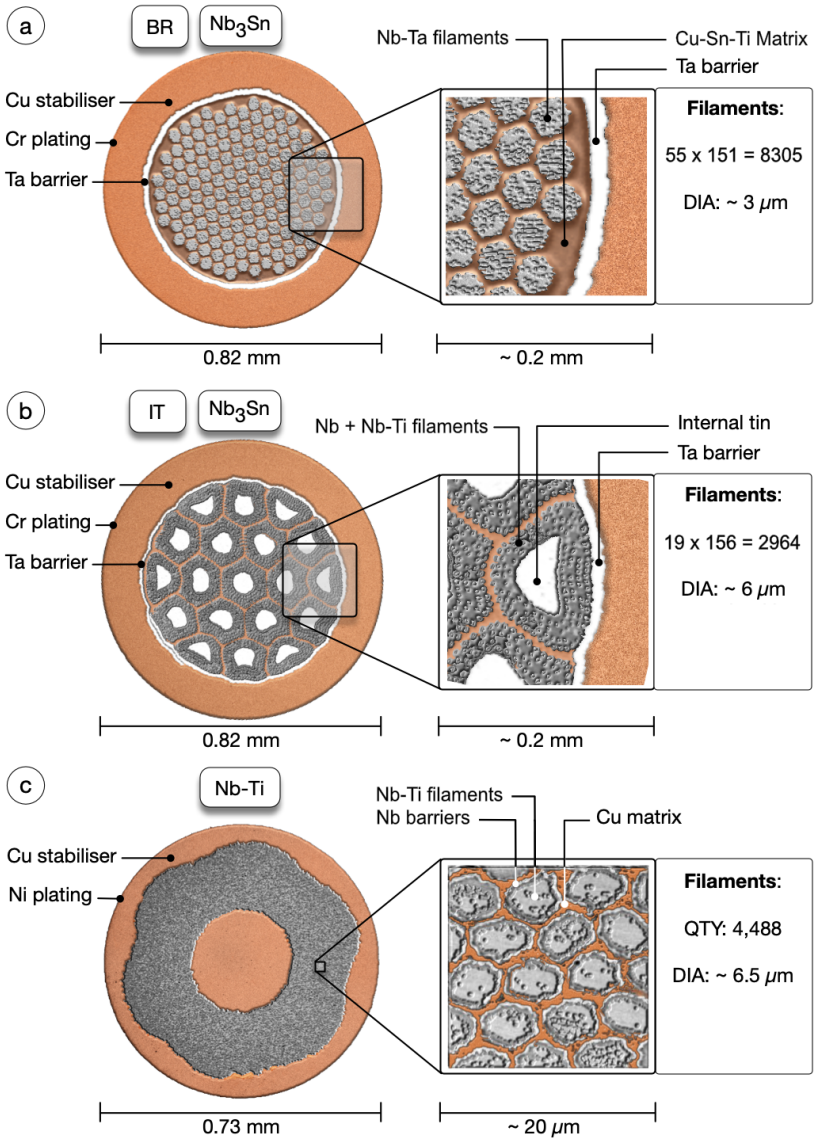

Figure 1: Strand architecture for ⓐ bronze route (BR) Nb_3Sn [17], ⓑ internal tin (IT) Nb_3Sn [17] and ⓒ Nb-Ti strand types [18]. The quantity and average diameters of the filaments are shown. The designations for the BR, IT and Nb-Ti strands were 01EE, 01EX and 11EC respectively.

2.3 Nb_3Sn Witness samples

The European Union's domestic agency (EUDA) was responsible for heat-treating (and fabricating) seven Nb_3Sn double pancakes (five regular and two side) for each of 10 TF coils in an exceptionally large furnace at ASG, Italy [5] - there are 18 TF coils in the final tokamak. Rather than rely entirely on thermometry located throughout the furnace to monitor temperature stability and homogeneity, it was decided that some strands that were representative of those included in the double pancakes would be cut from the relevant 25 m lengths and placed around each double pancake during each

Table 2: ITER specification values for the toroidal field coil Nb_3Sn and poloidal field coil Nb-Ti strands [5]. RRR: Residual Resistivity Ratio. For room temperature measurements, values in round brackets are the allowed range for the last digit. Plating thickness specification is between 1 µm and 2 µm.

	Both BR and IT Nb_3Sn		Nb-Ti	
	Conditions	Specification values	Conditions	Specification values
	Cryogenic measurements			
Critical current	4.22 K, 12.0 T [10 µV m^{-1}]	>190 A	4.22 K, 6.4 T [10 µV m^{-1}]	>306 A
n-value	10 µV m^{-1} to 100 µV m^{-1}	>20	10 µV m^{-1} to 100 µV m^{-1}	>20
RRR	273 K and 20 K	>100	at 273 K and 10 K	>100
Hysteresis losses	4.22 K and ±3 T	<500 mJ cm^{-3}	4.22 K and ±1.5 T	<55 mJ cm^{-3}
	Room temperature measurements			
Cu to non-Cu ratio		1.0 ± 0.1		1.55 to 1.75
Diameter		(0.820 ± 0.005) mm		(0.730 ± 0.005) mm
Twist pitch		(15 ± 2) mm		(15 ± 2) mm
Plating thickness	Chromium	$2, +0 - 1$ µm	Nickel	$2, +0 - 1$ µm

Table 3: Deliverable, strand, sample and measurement numbers: European Union Domestic Agency (EUDA) Nb_3Sn Internal Tin (IT) and Bronze Route (BR) Verification strands; Witness samples for the European Union (EU), United States of America (USA), China (CN) and Russia (RF) and Nb-Ti strands for Poloidal Field Coil 6. Critical current data obtained at three magnetic fields on one strand is considered one measurement.

	EUDA Nb_3Sn Verification strands			DA Nb_3Sn Witness samples					Nb-Ti	TOTALS
	IT	BR	TOTAL	EU	USA	CN	RF	TOTAL		
Deliverables received	17	17	34	1	1	1	1	4	1	39
Strands/samples received	2936	1041	3977	534	222	162	474	1392	323	5692
Heat-treatments in Durham	54	35	89	0	0	0	0	0	0	89
Original measurements made	6491	2454	8945	234	90	66	198	588	2571	12104
Additional measurements	651	63	714	0	0	0	0	0	0	714
Total strands/samples received										5692
Total measurements made										12818

heat-treatment to serve as witness samples. On receipt of the reacted samples back in Durham, about one third were selected for I_c measurements by the respective DA, as shown in Table 3, and the data compared against the original 25 m verification strand results to assess the heat-treatment quality. We note that all I_c values were sufficiently high and there was no evidence of heat-treatment problems during the witness samples campaign.

3 Nb_3Sn strand processing

3.1 Strand identification

Durham's strand preparation procedures met the requirements outlined in the F4E Technical Proposal [19]. On arrival, all strands were allocated unique four-digit Durham Reference numbers that were used to track the strands throughout their processing, measurement, reporting and storage. After the I_c barrels were manufactured, they were each engraved with a unique four-digit reference number allowing definitive strand identification. All personnel with access to the strands and barrels followed a strict code of practice that ensured strands could not be accidentally exchanged.

3.2 Furnaces and heat-treatment

Durham commissioned a suite of ten three-zone tube furnaces capable of continuous heat-treatments up to 1150 °C that were backed-up by an electrical generator. Each furnace was dedicated to a particular type of measurement; three (high purity furnaces) were allocated to residual resistivity ratio (RRR) strands, one for oxidisation of the titanium-alloy part of the critical current barrels and six to critical current (I_c) and hysteresis loss (Q) strands. Typically, 30 % were sequentially removed from service to conduct thermal rebalancing, thermocouple cross-checks and/or seal replacements. For RRR heat-treatments, where the highest purity environment was required, a Kanthal [20] (an iron-chromium-aluminium alloy) tube 1500 mm long and 90 mm diameter was used. The Kanthal allowed a stainless steel knife-edge sealing flange (used with a copper sealing ring) to be welded to one end of the tube while the other end was welded closed with a stainless-steel plate. Supelco Super Clean gas filters [21] were fitted to all gas inlets and an argon gas purity of six nines used. All exhaust outlets were fitted with bubblers and inline one-way valves to stop backflow into the furnaces. For each heat-treatment, zirconium foil was placed at both ends of the furnace tube to provide oxygen gettering [22]. In addition to the furnace manufacturer's control thermometry in the heating elements, Durham used three extra Type-N, Class 1, thermocouples (tolerance: −4.0 to +375 °C: ±1.5 °C; 375 to +1000 °C: ±0.4 %). One thermocouple was fitted in the central 600 mm region of the sample space and one in each of the outer heating zones. All thermocouples were continuously monitored throughout each heat-treatment. Additional thermocouples were purchased in batches and quality checked before use - for example, among a single group of six thermocouples, they would all be typically within 0.5 °C of each other at 395 °C. However, sometimes one would be an outlier at, say, ±2 °C and would be discarded. Temperature homogeneity of ±2 °C over the central 600 mm region of each furnace was improved by using alumina baffles at the ends of each furnace tube and surrounding the heat-treatment rigs with 600 mm long copper tubes. Each heating zone was kept within ±2 °C of the setpoint with a stability of ∼ ±0.2 °C.

After the furnaces were loaded with strands, they were pumped and flushed at least three times with argon gas. The heat-treatment schedule was specified by F4E [23–

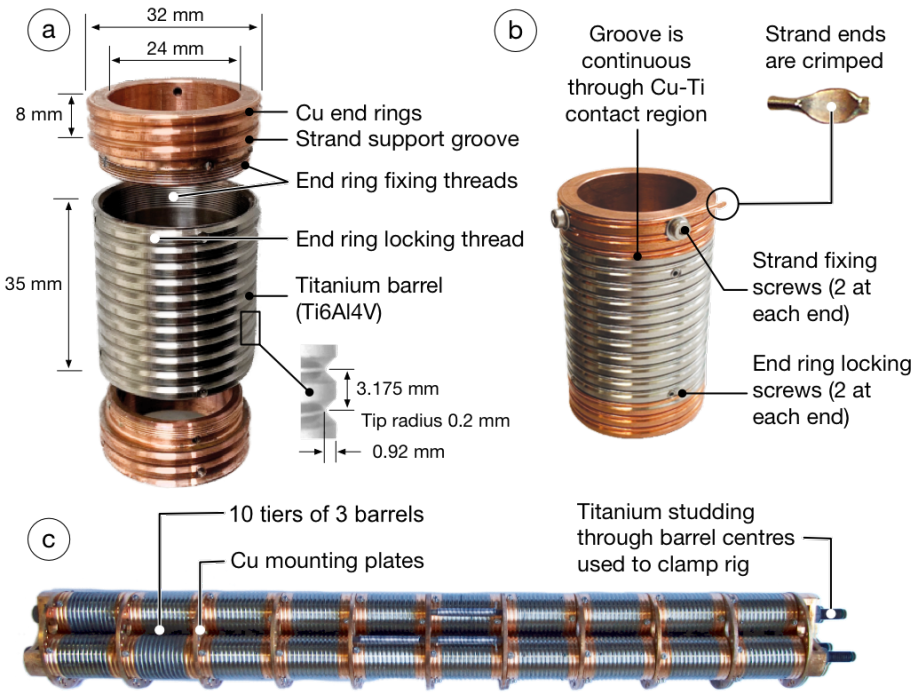

Figure 2: The Durham I_c barrel and heat-treatment rig; ⓐ disassembled view, ⓑ assembled view and ⓒ fully occupied heat-treatment rig. The heat-treatment rig also held hysteresis loss coils.

25]. The bronze route Nb_3Sn schedule contained two temperature plateaus of 595 °C (for 160 h) and 620 °C (for 320 h) while the internal tin Nb_3Sn schedule contained five temperature plateaus of 210 °C (for 50 h), 340 °C (for 25 h), 450 °C (for 25 h), 575 °C (for 100 h) and 650 °C (for 100 h). All ramp rates were at 5 ° h^{-1}. After the final plateau the temperature was decreased to 500 °C at which point the heaters were switched off and the furnace allowed to cool at a rate determined by ambient conditions.

3.3 Barrels and strand preparation

For the I_c measurements, Durham used bespoke ITER-type barrels (Figure 2) [26] where the end rings were adapted so they screwed onto the central titanium-alloy barrel and were locked in place with grub screws (reducing motion between the copper and titanium-alloy parts). Strand support was provided by a continuous groove over the entire length of the assembled barrel. After cleaning a manufactured barrel, the titanium-alloy part (alone) was oxidised in air at 300 °C for around 3 h to form a lubricated surface layer that inhibited strands from sticking to the barrels during heat-treatment.

Each strand had its chromium plating removed from the region over which it would be in contact with the copper end rings, either mechanically or by acid etching. It was then wound onto a barrel with a winding tension of 1 kg force (kgf) and fixed in place with screws at each end. For the internal tin Nb_3Sn strands the length of each strand

was extended beyond the screws by 30 mm so the ends could be crimped, impeding tin outflow during heat-treatment (Figure 2). After heat-treatment, the crimped ends were removed.

In preliminary RRR experiments, strands were reacted in flowing argon and produced RRR values that were artificially low. Changes were made following discussions with CERN: For each RRR measurement, each length of strand ~ 220 mm long was cleaned and placed inside protective quartz tubes (~ 4 mm outside diameter (OD) by ~ 1.5 mm inside diameter (ID) by 200 mm long). The close-fitting quartz tubes provided a barrier to the very low levels of oxygen in the flowing argon gas and produced visibly shinier strands [27]. After heat-treatment, a ~ 19 mm length was cut from the centre of each 200 mm strand and two small strips of chromium plating, ~ 7 mm apart, were delicately removed using fine grit Emery paper and voltage tap wires soldered in place using Pb-Sn solder.

For the hysteresis loss measurements, a 250 mm length of strand was wound onto a titanium-alloy rod to form a tight, supported, helical coil of approximately 60 turns with an outside diameter of ~ 5.7 mm. The ends of the coil were threaded through holes in the titanium-alloy rod to maintain the coil's shape during heat-treatment and were also crimped to impede tin leakage. The coils were then mounted alongside their corresponding I_c strands on the heat-treatment rig. After heat-treatment, the central 9 turns of each coil were cut from the 60 turn strands and their dimensions and mass (using a Mettler Toledo balance capable of measuring up to 81.0 g to within ± 0.005 mg) were measured. Usually, loss data are given per unit volume of superconductor. Here, we provide the loss per unit volume of the post-heat-treated strand (cf. Section 5.3).

4 Bespoke Critical Current Equipment

The activities associated with the processing and I_c measurements on the Nb_3Sn strands at 4.2 K were most of the work, both in terms of manpower and cost. Some important details of the equipment used to make the measurements are provided in this section.

4.1 External circuitry

A Power Ten 2000 A power supply was used to drive a linearly increasing current through a strand during an I_c measurement [28]. The output current of the Power Ten was measured using a Deltec standard shunt, calibrated to an uncertainty of ± 0.04 % - in this paper we have taken commercial calibration uncertainties to be 1 sigma. The voltage across the superconductor was amplified using EM Electronics DC nanovolt amplifiers (with 50k gains known to within ± 0.08 %). These amplifiers can make very low noise measurements, down to Johnson noise levels of a few nanovolts, associated with the resistance of the voltage tap leads. The amplifiers were connected to Keithley voltmeters capable of measuring to within 0.004 % of their input voltage and the experiment was controlled using a PC running a bespoke LabView data acquisition program.

4.2 Mounting strands on I_c-probes

After heat-treating the Nb_3Sn strands they were soldered to the copper end rings of their barrels using a hot-plate, a hot-air-gun and a soldering iron. During the initial phase of I_c measurements we found that the strands often quenched at relatively low electric fields. We associated this premature quenching with damage to the strand across the titanium-alloy barrel and copper end ring interface, possibly caused by the differential thermal contraction of the components of the strand and the barrel and the possibility of some strands sticking to the barrels during heat-treatment. Thereafter, we routinely soldered six short strap lengths ($\sim 15\,\mathrm{mm}$) of HTS tape (SuperPower SCS4050) across adjacent strand turns, bridging the copper-titanium interface around the circumference of each barrel. This increased the maximum electric field reached during measurements.

Typically, three barrels were mounted together in series onto one of the Durham I_c–probes, making a continuous electrical path through all three. The barrels were clamped together on the probe, forming solder-free push-fit copper-to-copper electrical contacts of cross sectional area (CSA) $\sim 350\,\mathrm{mm}^2$. Voltage tap wires were then soldered to each strand and non-inductively wound around the barrel, parallel to the length of the strand, to the point at which all three taps met [29, p 289]. They were then twisted to form a twisted-triplet of wires that were connected to the probe's voltage lead-throughs. The tap network consisted of two 250 mm series taps in parallel with one 500 mm tap. The voltages generated across different combinations of these three wires determined which of the three taps was measured. After the top strand had been measured, the probe was lifted in the magnet to position the next adjacent strand in field-centre. Up to 36 strands per week, with a team of two (and sometimes three) personnel, were regularly measured with a maximum (short term) capacity of 60 being possible in exceptional circumstances. Inevitably, a very small number of strands proved difficult to measure, which meant that none of the other strands on the probe could be measured. However, this was sufficiently unusual to ensure measuring three strands in series at a time was the more efficient choice.

Because the Nb-Ti strands are ductile and needed no heat-treatment, we designed a dedicated probe that allowed three strands to be wound directly onto it. The mounting procedure was similar to winding a strand onto a barrel except the lengths of the strand in contact with the copper rings (with nickel plating removed) were not soldered, but instead, clamped in place.

4.3 Temperature control and helium constraints

Large bubblers, fabricated in-house, were connected to the magnet Dewar with large-bore vacuum piping to keep the helium bath close to atmospheric pressure. They replaced mechanical one-way relief valves that were prone to sticking. Atmospheric pressure data were obtained from a publicly accessible local weather station [30] to determine the difference in helium bath temperature from 4.22 K each day [28].

During the contract Durham and many other laboratories were hit by a global

liquid helium shortage. Our supplier reduced helium deliveries to 80 % of our previous year's average monthly usage [31, 32], which threatened our delivery schedule. Following detailed calculations [32] we reduced the cross-sectional areas of the current leads by ~ 44 % and ran the probes hot, successfully reducing the helium usage per strand by over 20 %.

4.4 Magnetic field

Durham used its 15 T vertical magnet to make all in-field I_c measurements. It has a 40 mm bore diameter and is homogeneous to 10^{-3} over a 10 mm diameter sphere volume. The field profile of the magnet was checked using an NMR calibrated Hall sensor. Small field-dependent corrections were applied to adjust for the strand being radially displaced within the magnet bore (i.e. at the radius of the barrel, ~ 16 mm). For example, when the magnetic field in the centre of the magnet bore was set to 11.968 T, along the length of the strand, the average field was 12 T and the variation in field $\pm$ 12 mT.

5 Cryogenic measurements, cross-checks and estimated errors/uncertainties

In this section and the next, we provide estimates for the standard deviation, normalised by the Durham mean value ($\bar{x}_{Dur,\,Raw}$), of both the random ($\tilde{\sigma}_{Est,\,Rand}$) and systematic ($\tilde{\sigma}_{Est,\,Syst}$) lab errors introduced during the processing-and-measurement in Durham.

5.1 Critical current (I_c) and index of transition (n-value) at 4.2 K

For Nb_3Sn strands, I_c (and n-value) measurements at 4.22 K in three applied magnetic fields, 12.5, 12.0 and 11.5 T were required. Before the start of each measurement sequence, the field was lowered to 10 T and the relevant strand centred. For Nb-Ti, the field values were 7.0, 6.4 and 6.0 T. For both materials, the field was set to 0.5 T above the highest required field and the measurements were then made from high field to low field. Each I_c measurement took ~ 2 min.

We investigated several sources of error: In preliminary experiments, we measured fifteen different IT Nb_3Sn strands that were then warmed to room temperature, and then repeat measurements made to investigate the effect of thermal cycling. An increase in the average I_c of 0.6 % was observed in the repeat measurement data. Such an increase has been reported before by Goodrich *et al.* who found thermally cycling strands increased I_c by up to 1 % at 12 T [33], which is most likely caused by strain relaxation of the filaments. We also measured groups of three strands in different positions on the probes and found, consistent with the strands being well supported by the barrels and in direct contact with the liquid helium, no evidence for damage, heating, or cross-talk between them, except in exceptional circumstances when there was a very marked increase in helium boil-off associated with one of the strands quenching. We also investigated to what degree the uniformity of the temperature in the furnaces

introduced random errors during the heat-treatments. We found that a change from 650 °C by 2.6 °C in the final heat-treatment temperature, which is the tolerance of the thermocouples at that temperature, led to a change in I_c of the IT strands of $\sim 1\,\%$; Data collected over a two-year period showed that in Durham fluctuations in ambient pressure produced variations in the helium bath temperature equivalent to an uncertainty of $0.3\,\%$ in I_c for both internal tin and bronze route Nb_3Sn so no temperature corrections were made. For Nb-Ti, Durham applied a helium bath temperature correction to account for deviations away from 4.2 K in accordance with the F4E technical document [34]. Typical corrections were ~ 10 mK, equivalent to $\sim 0.2\,\%$ in I_c; The instrumental uncertainty in Durham's I_c measurements is estimated to be small, $\sim 0.1\,\%$.

Our best estimate of the random errors introduced by processing-and-measurement of I_c are $\sim 1.5\,\%$ and $\sim 1.0\,\%$ for the Nb_3Sn and Nb-Ti strands, respectively. The equivalent systematic errors are estimated to be $\sim 1.5\,\%$ and $\sim 0.5\,\%$. Equally, the empirical relation between I_c and n-value can be written in the form

$$\frac{dn}{n}/\frac{dI_c}{I_c} \approx s\,, \tag{5}$$

where $s \approx 0.4$ [35]. However, we estimate the random errors for the n-value data to be larger than those of I_c, $\sim 2.0\,\%$ and $\sim 1.5\,\%$ for the Nb_3Sn and Nb-Ti strands and equivalent systematic values to be $\sim 1.5\,\%$ and $\sim 0.5\,\%$, as shown in Tables 4 to 7. The uncertainties in I_c are dominated by variations in the homogeneity of the furnaces, but the n-values have additional contributions from the (non-zero) base-line and non-power law behaviour in the I-V characteristics, symptomatic of filament damage and thermal voltages [28]. Although the sensitivity of brittle Nb_3Sn to handling may contribute to the total uncertainty, since we have no good way to quantify the random and systematic errors that result, we simply note that great care was taken with handling the strands and that there is no contribution from damage to the strands from handling that is specifically included in our estimated errors. Some scanning electron microscopy (SEM) suggests that the internal tin architecture is substantially more susceptible to crack formation than the bronze route architecture [36]. Similarly, the purity of the gas environment and rupture of the Ta diffusion barrier during heat-treatment are also an unquantified possible source of error. The approach in this paper is to set the lab errors associated with handling and barrier rupture to zero, and consider them as candidate unidentified errors in any of the random or systematic lab errors. Similarly, we set all the systematic lab errors associated with gas purity, that can lead to differences in the averages between the two labs in any of the cryogenic data (n.b. we do not know the final gas purity during the heat-treatment in either Durham or the manufacturer's lab), to be zero. For the random errors, however, we made measurements of the average of several strands reacted in high purity and low purity gas environments to estimate and include the effects of gas purity on the RRR and Q measurements in Durham, but have not explicitly included a random error associated with gas purity for I_c or n-value (or any of the room temperature measurements) where the effects of gas purity are expected

to be negligible.

5.2 Residual resistivity ratio, RRR

The Durham RRR probes held ten strands (nine verification strands and one Nb-Ti "standard" strand that remained on the probe to measure reliability). A commercially calibrated CERNOX thermometer was also attached to the strand platform to improve temperature accuracy and the base of the platform was fitted with a blank PPMS puck to allow good, direct, thermal contact to the Quantum Design Physical Property Measurement System (PPMS) that was used for temperature control. At 273 K, a typical offset between the control and calibrated thermometry was −1 K. The offsets for Nb_3Sn (at 20 K) and for Nb-Ti (at 10 K) were between −2.3 K to −1.5 K depending on which probe was being used. High precision circuitry, external to the PPMS, was used to make the RRR measurements, including a calibrated Keithley current source and 10 EM Electronics nanoamplifiers. The measurement sequence comprised of driving 100 stepped polarity-reversed currents (to cancel thermal voltages) in the range 0 to 100 mA through all ten RRR strands while measuring the voltage response of each. A suite of six RRR probes gave a measurement capacity of ∼135 strands per week.

In initial experiments, ten strands were sequentially measured in different positions (and different sides) on the sample platform and found to vary by less than 0.5 %. Consistent with this result, we find the error associated with the RRR measurements to be small: The main sources of random error are temperature setpoint accuracy, stability, and uniformity of temperature along the strand platform. We measured the temperature dependence of the resistivity of the strands (predominantly the copper) at 273 K to be $\sim 0.4\,\%\,\mathrm{K}^{-1}$ and that at 20 K to be $\sim 2.8\,\%\,\mathrm{K}^{-1}$[29, p 242]. The uncertainty in the temperature setpoint of the PPMS at 273 K was 0.04 % and at 20 K was 0.4 %, which leads to random errors in RRR of ∼0.2 %. We estimate the systematic errors from the instrumental uncertainties to be 0.5 %.

In a blind cross-check between Durham, the manufacturer, CERN, and another laboratory, ten IT strands were simultaneously heat-treated by CERN and then split and measured by Durham and the other laboratory. The measurement results were similar to each other to within ∼1 %. However, the average RRR of the strands heat-treated by Durham was 7 % higher than those heat-treated at CERN and 8 % lower than those heat-treated by the manufacturer. This confirms that most of the lab errors in RRR are associated with the gas purity (and/or gas type) and the uniformity of the temperature during the heat-treatment. During this work it was demonstrated that heat-treating in nitrogen produces a systematic increase in RRR of ∼25 %, probably caused by nitrogen bonding to electronic scattering sites in the copper [37]. Following discussions with CERN we placed all strands inside small protective quartz tubes which increased RRR. All RRR measurements reported in this paper are for Nb_3Sn strands placed in small quartz tubes and heat-treated in high purity argon.

We conclude that for Nb_3Sn, the differences in RRR observed between partner labs

were predominantly associated with different heat-treatment gas purity and that its effect is different for bronze route and internal tin strands. Using high purity argon gas in both labs reduced the differences, but it is clear that direct measurement and control of the gas impurity concentrations would further reduce random and systematic errors in our data (also for RRR and Q losses as discussed below). Such improvements have to be weighed against increased cost and technical requirement to check the strand/magnet performance is not too sensitive to heat-treatment conditions. For the strands heat-treated in Durham, we estimate the RRR random lab error to be $\sim 2\,\%$ and the systematic error to be $\sim 1.0\,\%$, while recognising that in the latter case, gas purity is not quantified and may lead to systematic differences between the two labs. For the Nb-Ti strands where there is no heat-treatment, we estimate both the random and systematic errors to be $\sim 1.0\,\%$.

5.3 Hysteresis loss, Q

The reacted 9 turn Nb_3Sn and Nb-Ti coils were inserted into straws and measured at 4.22 K in the field range ± 3 T and ± 1.5 T, respectively. The applied field was swept at a rate of $4\,\mathrm{mT\,s^{-1}}$. The losses per unit volume were calculated using a mass measurement of the strand and the post-heat-treated density of the Nb_3Sn strands. Twelve 240 mm long straight strands were measured before and after heat-treatment. The change in average elongation was found to be small: $\pm 0.3\,\%$. The internal tin strand diameters increased by $(1.3 \pm 0.2)\,\%$ whereas the bronze route strands increased by just $(0.4 \pm 0.1)\,\%$. These corrections follow from the elemental niobium and tin being converted into Nb_3Sn and voids (Kirkendall voids [38–41]) during the heat-treatment. Our 9 T PPMS was used in Dc-extraction mode to make the hysteresis loss measurements (where the sample is slowly moved between pick-up coils rather than oscillated [42, 43]), and periodically calibrated using a 3.1 mm diameter by 3.9 mm long standard cylindrical block of palladium.

Several cross-checks were conducted: Five successive losses measurements were made on a strand cut down from thirteen turns to nine and an increase of 3 % found, consistent with finite-sized pick-up coils [44]. A batch of ten strands was prepared and heat-treated by Durham and another set of ten strands, from the same batch, prepared and heat-treated by the manufacturer. Both sets of heat-treated strands were then measured by Durham and NIST (National Institute of Standards and Technology, USA). The difference in the mean values of the measurement results (alone) for each strand batch was 3 % and 4 % respectively. Durham also sent one heat-treated strand coil to another lab for re-measurement and the results agreed with Durham's to within 1.8 %. We also checked whether the purity of gas in the furnaces affected the loss measurements by heat-treating twelve IT strands in one of the high-purity (RRR) furnaces and comparing them to strands heat-treated alongside the I_c strands in one of the lower purity furnaces. An average reduction of $\sim 4\,\%$ was observed in those strands heat-treated in the higher purity furnace. As with the RRR measurements, we conclude

that the loss measurements are sensitive to the processing gas purity. Given that the IT strand losses are affected by gas purity, which suggests that gas purity can affect the superconducting material inside the Ta diffusion barrier, it opens the possibility that gas purity also may affect the I_c and n-value data. There are several other sources of random and systematic error in the hysteresis loss measurements but they are relatively small, associated with the accuracy and stability of the setpoint temperature ($\sim 2\,\mathrm{mK}$) and the dB/dt inductive contribution.

We expect the main sources of random lab errors for the Nb_3Sn strands to come from furnace inhomogeneity and variation in gas purity and to be $\sim 2\,\%$. For the Nb-Ti strands, we expect the random error to be about $0.5\,\%$, predominantly associated with the strand centring and the measurement error of the physical size of the strand. Although there is the uncertainty in the Nb_3Sn strand density of $\sim 0.5\,\%$, the difference in physical size of the strands and the standard palladium sample used to calibrate the equipment is expected to give the largest systematic error contribution, estimated to be $\sim 2\,\%$ for both Nb_3Sn and Nb-Ti. However, we also note that as with the RRR measurements, we expect additional systematic differences in the losses between Durham and manufacturer, associated with different gas purity in the two labs during the respective heat-treatments.

6 Room temperature measurements and estimated errors

Strands were cleaned with isopropanol prior to all room temperature measurements.

6.1 Copper to non-copper ratio, CnC

For the Nb_3Sn strands, scanning electron microscope images of strand cross-section were obtained using Durham's Hitachi SU-70 FEG, measuring up to 36 strands at a time. Images were analysed in Adobe Photoshop and the cross-sectional areas occupied by the copper and the non-copper regions were measured. The dominant random errors are associated with the SEM image resolution and working within Photoshop. We estimate both the random and systematic errors to be $\sim 1\,\%$.

For Nb-Ti strands, a 30 to 40 mm length was cut and the average of four mass measurements taken. The strand was then fully etched in 30 % nitric acid until only loose Nb-Ti filaments remained. The filaments were then removed from the acid and allowed to air dry. After drying, their combined mass was measured, and the copper to non-copper ratio calculated using the length of the strand, the diameter of the strand, the change in the mass of the strand after etching and the density of copper. We did not include the small correction from the mass of the nickel plating. In initial small quantity experiments, 24 adjacent strands were measured in Durham and another lab and good agreement to $\leq 1\,\%$ was found. We estimate the Durham random and systematic errors to be $\sim 0.1\,\%$.

6.2 Strand twist pitch, T_P

For Nb_3Sn strands, the central 30 mm region of a $\sim$100 mm strand length was etched down to the tantalum barrier using 30 % nitric acid for $\sim$15 min revealing striations caused by the underlying filament bundles. For Nb-Ti, a short length of strand was submerged in 30 % nitric acid for a few minutes to expose the underlying filaments. The etching was stopped after the filaments at the surface were exposed, retaining enough copper matrix to maintain both the structural integrity of the pre-etched strand and the twist pitch of the filaments. Then the etched strands were photographed using a fourteen megapixel digital camera (with $\times$10 magnification), and were analysed in Adobe Photoshop. The twist pitch was calculated using the etched strand's diameter, and the angle that the filaments made with the axis of the strand. ITER's acceptance criteria (Table 2) specified that the twist pitch only had to be measured to an uncertainty of 13 %. We estimate the random errors in our measurements to be $\sim$8 % and have taken the confidence level of the random error from measuring the 116 strands (i.e. $8\,\%/\sqrt{116}$) as a rough upper bound estimate for our systematic error, $\sim$1 %. During the contract period, Durham found two twist-pitch outliers: two strands had a twist pitch half that of the specified value as a result of being twisted twice during manufacture. They were rejected for use in the TF coils and not included in our analysis.

6.3 Strand diameter, S_D

The diameter of the Nb_3Sn and Nb-Ti strands were both measured using a Scantron Dual-axis Laser Micrometer. An average of ten circumferential measurements at four different locations along a strand length was obtained. The Laser micrometer can measure wire diameters in the range 0.03 to 3.0 mm, with a resolution of 0.01 µm. In initial small quantity experiments on 12 strands, Durham and a third lab found excellent agreement to $\leq$0.2 %. The estimated Durham random error is $\sim$0.1 %. The calibration of the micrometer was periodically checked using four stainless steel precision gauges [45] with diameters in the range 0.800 to 0.830 mm (each with tolerance +0.001 mm). These gauges were stored in a dry inert atmosphere to maintain diameter/surface quality. We estimate the systematic error in Durham to be $\sim$0.1 %.

6.4 Plating thickness, P_T

In preliminary experiments on the chromium-plated Nb_3Sn strands, we used our scanning electron microscope facility to measure the average plating thickness P_T at six locations around the circumference of each strand, separated by 60 degrees. Strands first had to be electroplated with copper to maintain the integrity of the chromium plating during strand preparation (polishing). This method was machine and labour intensive. Subsequently (for the vast majority of measurements), we used a mass measurement approach. We first cleaned 1000 mm long strands with acetone to remove any surface grease/dirt. The mass of each strand was then measured four times and an average

taken. The chromium plating was then acid etched away with dilute hydrochloric acid (37 %) for a few minutes and another mass measurement made. The plating thickness was then calculated from the change in mass, the average strand diameter (with chromium), the strand length and the known density of chromium and the associated errors added in quadrature to give a random error of 0.1 %. A small quantity comparison between twelve pairs of adjacent strands measured in Durham and elsewhere gave a difference of 8 %. Our estimated systematic error is $\sim$0.1 %, predominantly associated with an uncertainty in the density of the plated chromium.

For the Nb-Ti strands, a $\sim$60 mm strand length was placed in a commercially available Fischer Instrumentation CM2 Couloscope using electrolyte type F6. The equipment used an electrical current driven deplating electrolysis process, measuring 40 mm of a 60 mm length of strand. The nickel plating thickness was calculated using the manufacturer's electrochemical parameter (the mass of a substance transported by one Coulomb of charge), the deplating current, the current efficiency (determined during manufacturer calibration of the equipment), the surface area of the strand, the known density of nickel, and the deplating time [46]. We estimate that both the random and systematic errors from the Couloscope measurements are $\sim$0.3 %.

7 Statistical analysis of the IT Nb_3Sn I_c and n-value data

7.1 Variables, terminology and analysis of raw measurements

In this section we focus on a subset of the Durham data shown in Table 4, namely the I_c measurements at 12.0 T on the IT strands, as a way of systematically defining the variables used in this paper/Table 4, and introducing the terminology for all the measurements.

As discussed in sections 5 and 6, we estimate the standard deviation of both the random ($\tilde{\sigma}_{Est\,Rand}$) and systematic [$\tilde{\sigma}_{Est\,Syst}$] lab errors in Durham to be 1.5 %, and the dominant source of those errors to be variations in the heat-treatment (HT). The two strand numbers given are those strands measured by Durham for which there were corresponding manufacturer's data available (i.e. 980), as well as the total number of strands measured in Durham (i.e. 1065). The I_c dataset is a compilation of subsets of data that belong to one of 17 strand deliverables shown in Figure 3 ⓒ.

The average values of I_c ($\bar{x}_{Dur,Raw}$ and $\bar{x}_{Man,Raw}$) were 275.7 A and 282.4 A for Durham and the manufacturer. The systematic difference ($\Delta\bar{x}_{Raw}$) between the averages of the Durham and manufacturer datasets is -2.4 %, where for simplicity and clarity, all data in this paper that are percentages carry a tilde in their variables to denote they have been normalised by the Durham mean value ($\bar{x}_{Dur,Raw}$). This convention leads, for example, to a normalised standard deviation (NSD) that is similar to the Coefficient of Variation in that they are both dimensionless (CoV - defined as the ratio of the standard deviation to the mean of each specific distribution [47]), but avoids any ambiguity about which mean has been chosen for those variables that are derived using data from both

labs (e.g. $\tilde{\sigma}_{P.Lth,\,Raw}$ and $\tilde{\sigma}_{\Delta,\,Adj}$ below), retains the simple form of the sum of variances law (cf. Eqns. (8) and (9) below), and avoids the standard problem of very large values of CoV occurring when the average of the distribution is zero or close to zero. In the first block of data in Table 4, variables are derived from the raw data and have the subscript 'Raw'. The raw I_c data from Figure 3 ⓐ have a NSD for each laboratory ($\tilde{\sigma}_{Dur,\,Raw}$ and $\tilde{\sigma}_{Man,\,Raw}$) given in Table 4 of 6.2 % and 5.3 % respectively. The two raw datasets are replotted in Figure 4 ⓐ as histograms. In these histograms, those strands that have I_c values greater than 300 A are identified, as well as the adjacent strand in the equivalent manufacturer's data. There is a strong correlation between the adjacent strands, such that a strand with high I_c tends to have an adjacent strand with high I_c. The NSD of the raw measurements from Durham (i.e. $\tilde{\sigma}_{Dur,\,Raw}$) shown in Figure 4 is given by

$$\tilde{\sigma}^2_{Dur,\,Raw} = \tilde{\sigma}^2_{Dur,\,Dtd,\,Raw} + \tilde{\sigma}^2_{P.Lth,\,Raw}\,. \tag{6}$$

The subscript 'Dtd' represents from 'Door to data', which includes all processing (handling, heat-treating and preparation) and measuring in the laboratory. We denote the NSD of the random lab error introduced in the Durham lab as $\tilde{\sigma}_{Dur,\,Dtd,\,Raw}$. The variable $\tilde{\sigma}_{P.Lth,\,Raw}$ is the NSD of the piece-length ends (i.e. the piece-length variability) derived from the raw data. Similarly, for the manufacturer,

$$\tilde{\sigma}^2_{Man,\,Raw} = \tilde{\sigma}^2_{Man,\,Dtd,\,Raw} + \tilde{\sigma}^2_{P.Lth,\,Raw}\,. \tag{7}$$

Comparing Figure 4 ⓐ and Figure 4 ⓑ shows, as expected, that the correlation between the high I_c data is reduced after the smoothing is complete. Equations 6 and 7 are similar to Eqs. 1 and 3. As discussed in the introduction, the values of $\tilde{\sigma}_{Dur,\,Dtd,\,Raw}$ (and $\tilde{\sigma}_{Man,\,Dtd,\,Raw}$) can be estimated by the scientists, using for example the known accuracy of their instruments or the uniformity of their furnaces (as we have above), and then the normalised standard deviation of the strands ($\tilde{\sigma}_{P.Lth,\,Raw}$) calculated. This approach can be thought of as trying to solve these two equations with three unknowns - which cannot be done without introducing (one or two of) the estimated lab error values. Repeat measurements on a single strand would in principle provide a measured value of the lab errors that can replace the estimated values, but it is clearly not possible here where each lab independently processses and measures its own strands.

Table 4: Critical current and n-value analysis using data from Durham and from the manufacturer for IT Nb_3Sn showing the effect of subtracting a moving average from the raw data (subscript: Raw) using different smoothing window sizes from 10 to 80 to produce smoothed data (subscript: Smd). The abbreviations used are I_c: critical current; n-value: index of transition. The variable $\tilde{\sigma}_{MA}$ [in square brackets] is the normalised standard deviation of the moving average. The variables used in this Table are defined in Section 7.1. The dashes denote non-physical (negative variance) values.

		I_c at 12.0 T		n-value	
Units		A		Dimensionless	
Estimated random [systematic] error.		1.5%, [1.5%]		2.0%, [1.5%]	
Dominated by		HT		HT	
Laboratory		Dur	Man	Dur	Man
Strand number: Both labs ,[Durham]		980, [1065]		980, [1065]	
$\bar{x}_{Lab}$	(Various)	275.7	282.4	36.1	39.1
$\Delta\bar{x}$	(%)	−2.4		−8.5	
$\tilde{\sigma}_{Lab,\,Raw}$	(%)	6.2	5.3	13.0	15.9
$\tilde{\sigma}_{\Delta,\,Adj}$, $[\tilde{\sigma}_{\Delta,\,Rand,\,Raw}]$	(%)	4.1, [8.2]		15.5, [20.5]	
$\tilde{\sigma}_{Lab,\,Dtd,\,Raw}$	Max(%)	3.7	1.8	8.8	12.7
	Min (%)	3.5	1.5	2.0	9.4
$\tilde{\sigma}_{P.\,Lth,\,Raw}$	Max (%)	5.1		12.8	
	Min (%)	5.0		9.5	
		Smoothed analysis after moving average subtracted			
Window size:		**80**			
$\tilde{\sigma}_{Lab,\,Smd}$	(%)	4.0	4.1	8.7	14.4
$\tilde{\sigma}_{\Delta\,Adj}$, $[\tilde{\sigma}_{\Delta,\,Rand,\,Smd}]$	(%)	4.1, [5.8]		15.5, [16.8]	
$\tilde{\sigma}_{Lab,\,Dtd,\,Smd}$	Max (%)	2.8	3.0	7.4	13.6
	Min (%)	1.5	1.7	2.0	11.6
$\tilde{\sigma}_{P.\,Lth,\,Smd}$, $[\tilde{\sigma}_{MA}]$	Max (%)	3.7,		8.5,	
	Min (%)	2.8, [4.0]		4.6, [7.9]	
Window size:		**40**			
$\tilde{\sigma}_{Lab,\,Smd}$	(%)	4.0	4.2	8.5	14.2
$\tilde{\sigma}_{\Delta\,Adj}$, $[\tilde{\sigma}_{\Delta,\,Rand,\,Smd}]$	(%)	4.1, [5.7]		15.5, [16.6]	
$\tilde{\sigma}_{Lab,\,Dtd,\,Smd}$	Max (%)	2.8	3.0	7.4	13.6
	Min (%)	1.5	2.0	2.0	11.5
$\tilde{\sigma}_{P.\,Lth,\,Smd}$, $[\tilde{\sigma}_{MA}]$	Max (%)	3.7,		8.2,	
	Min (%)	2.9, [4.2]		4.1, [8.4]	
Window size:		**20**			
$\tilde{\sigma}_{Lab,\,Smd}$	(%)	3.7	4.0	8.4	13.9
$\tilde{\sigma}_{\Delta\,Adj}$, $[\tilde{\sigma}_{\Delta,\,Rand,\,Smd}]$	(%)	4.1, [5.4]		15.5, [16.3]	
$\tilde{\sigma}_{Lab,\,Dtd,\,Smd}$	Max (%)	2.7	3.1	7.7	13.5
	Min (%)	1.5	2.1	2.0	11.3
$\tilde{\sigma}_{P.\,Lth,\,Smd}$, $[\tilde{\sigma}_{MA}]$	Max (%)	3.4,		8.2,	
	Min (%)	2.5, [4.3]		3.4, [8.8]	
Window size:		**10**			
$\tilde{\sigma}_{Lab,\,Smd}$	(%)	3.5	3.7	8.0	13.1
$\tilde{\sigma}_{\Delta\,Adj}$, $[\tilde{\sigma}_{\Delta,\,Rand,\,Smd}]$	(%)	4.1, [5.1]		15.5, [15.4]	
$\tilde{\sigma}_{Lab,\,Dtd,\,Smd}$	Max (%)	2.8	3.0	-	-
	Min (%)	1.5	1.9	-	-
$\tilde{\sigma}_{P.\,Lth,\,Smd}$, $[\tilde{\sigma}_{MA}]$	Max (%)	3.2,		- ,	
	Min (%)	2.1, [4.5]		- , [-]	

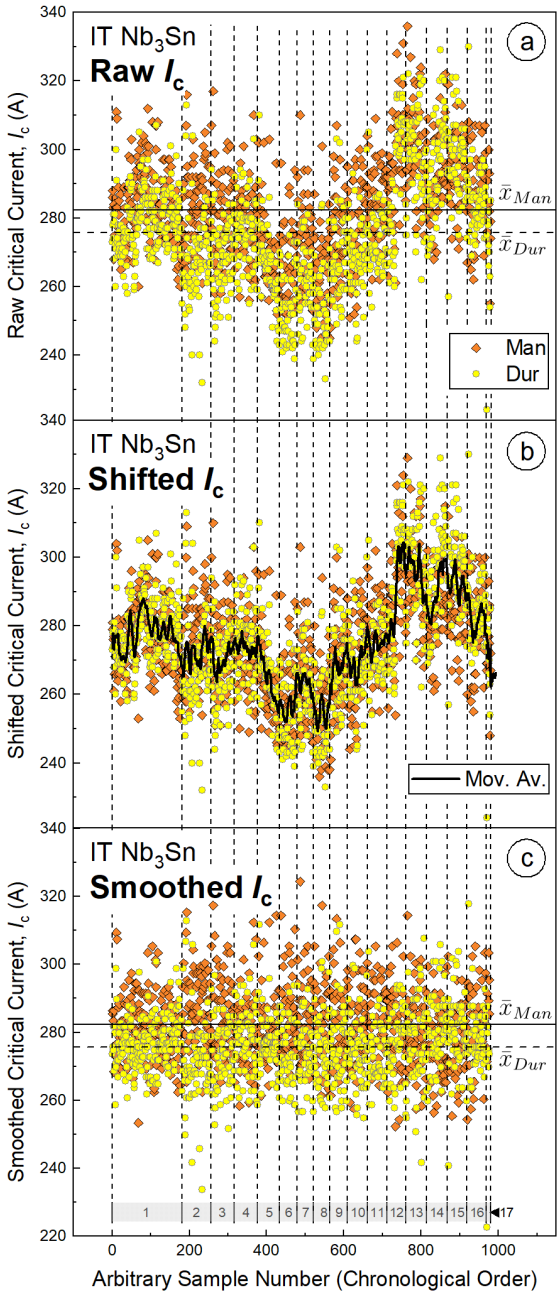

Figure 3: The Durham (Dur) and manufacturer (Man) I_c data for the internal tin (IT Nb_3Sn) strands in chronological order. ⓐ Raw data, ⓑ a 20-point moving average (MA) of the Durham data and the manufacturer data after the latter has been shifted to the Durham mean and ⓒ the smoothed data for both labs after subtracting the MA from the raw data and the mean of the manufacturer data has been restored. The strands received by Durham were grouped into 17 individual deliverables represented here by vertical dashed lines.

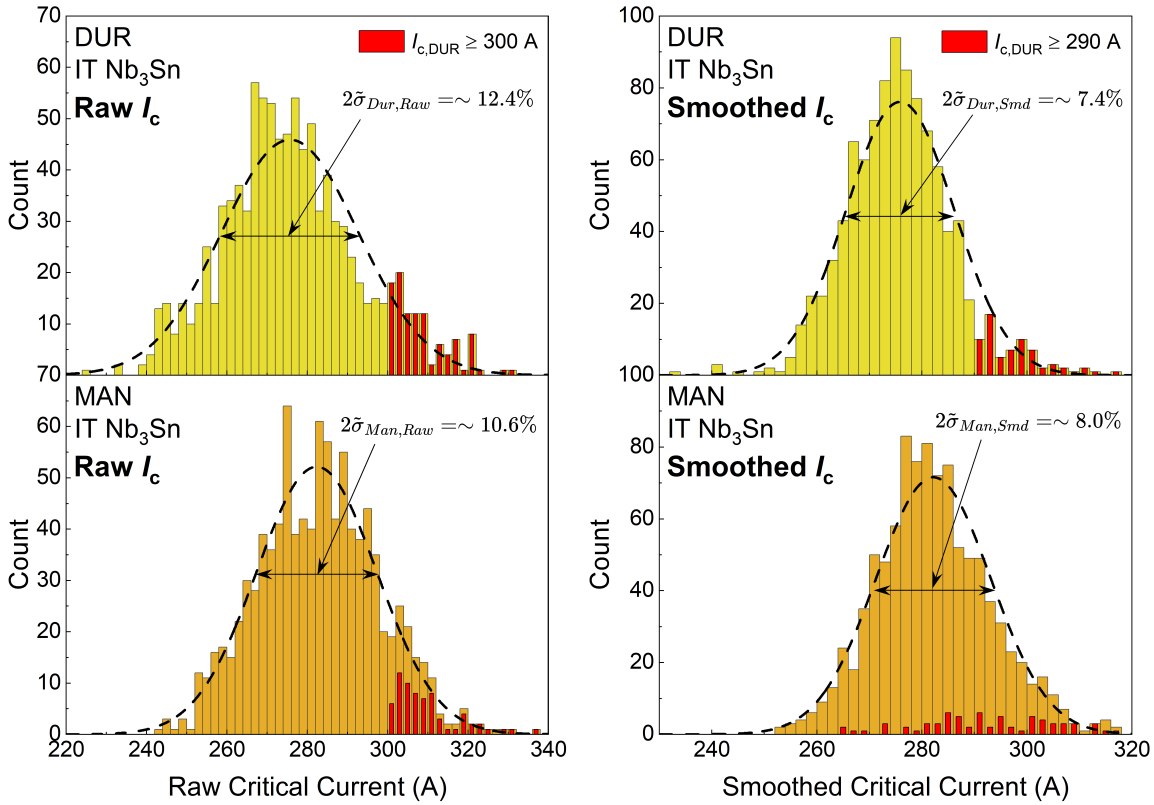

Figure 4: The normal distributions (black dashed lines) for the Durham (Dur) and manufacturer (Man) internal tin (IT Nb_3Sn) I_c data. ⓐ raw data distributions and ⓑ smoothed data obtained after subtracting the 20-point moving average from the raw data. The red bars identify those Durham strands with high I_c's, together with their associated adjacent strand data from the manufacturer.

Figure 5 shows how the component variances add to give the variance of the difference between the measurements on adjacent strands from Durham and the manufacturer, which is denoted by $\tilde{\sigma}_{\Delta,\,Adj}$ and the separation of the two squares. Table 4 shows for the I_c measurements, $\tilde{\sigma}_{\Delta,\,Adj} = 4.1\,\%$. The separation of the two circles denotes the variance of the difference in the properties of adjacent strands, where the associated NSD is $\tilde{\sigma}_{Adj,\,Corr}$. There are three cases shown: ⓐ adjacent strands are as uncorrelated as the piece-length ends; ⓑ the general case where adjacent strands are partially correlated; and ⓒ, adjacent strands are perfectly correlated (i.e. adjacent strands have identical properties) with the circles on top of each other. In all three panels ⓐ to ⓒ, the variance of the measurements in Durham $\sigma^2_{Dur,\,Raw}$ (and similarly the manufacturer), equals the sum of the variance of the ends of the piece-lengths $\sigma^2_{P.Lth,\,Raw}$ and the variance introduced by the laboratory from door-to-data $\sigma^2_{Dur,\,Dtd,\,Raw}$ (cf. Eqs. 6 and 7). It is unaffected by the degree to which adjacent strands are correlated. In panel ⓐ, $\sigma^2_{Adj,\,Corr}$ has its maximum possible value. The variance of the difference of the measurements on the adjacent strands $\sigma^2_{\Delta,\,Adj}$ also has its maximum possible value. In

panel ⓒ, the adjacent strands are identical so $\sigma^2_{Adj,\,Corr} = 0$, and $\sigma^2_{\Delta,\,Adj}$ has its minimum value. Panel ⓑ shows the general case where adjacent strands are partially correlated and Eq 4 can be generalised (and normalised) to

$$\tilde{\sigma}^2_{\Delta,\,Adj} = \tilde{\sigma}^2_{Adj,\,Corr} + \tilde{\sigma}^2_{Dur,\,Dtd,\,Raw} + \tilde{\sigma}^2_{Man,\,Dtd,\,Raw}\,. \tag{8}$$

Were the pairs of strands measured by each verification lab to be randomly selected (rather than being adjacent to each other), the variance sum rule for the variance of the difference in the values of I_c ($\tilde{\sigma}_{\Delta,\,Rand,\,Raw}$) gives Bienayme's identity where,

$$\tilde{\sigma}^2_{\Delta,\,Rand,\,Raw} = \tilde{\sigma}^2_{Dur,\,Raw} + \tilde{\sigma}^2_{Man,\,Raw}\,. \tag{9}$$

Table 4 includes the value of $\tilde{\sigma}_{\Delta,\,Rand,\,Raw} = 8.2\,\%$ [in square brackets], calculated from pairing each measurement of I_c in the Durham dataset with all possible choices from the manufacturer dataset (approximately $\approx 10^6$ datapoints). Although the I_c data are not perfect normal distributions, the values calculated for $\tilde{\sigma}_{\Delta,\,Rand,\,Raw}$ agree with calculations using Eqn. 9 to much better than 1 %. Equation 9 follows from random selections from two normal distributions and contains no new information about the component variances that appear on the right-hand side (RHS) of the equation - consistent with the sum of the RHS of Eqns 6 and 7 being equal to the RHS of Eqn. 9.

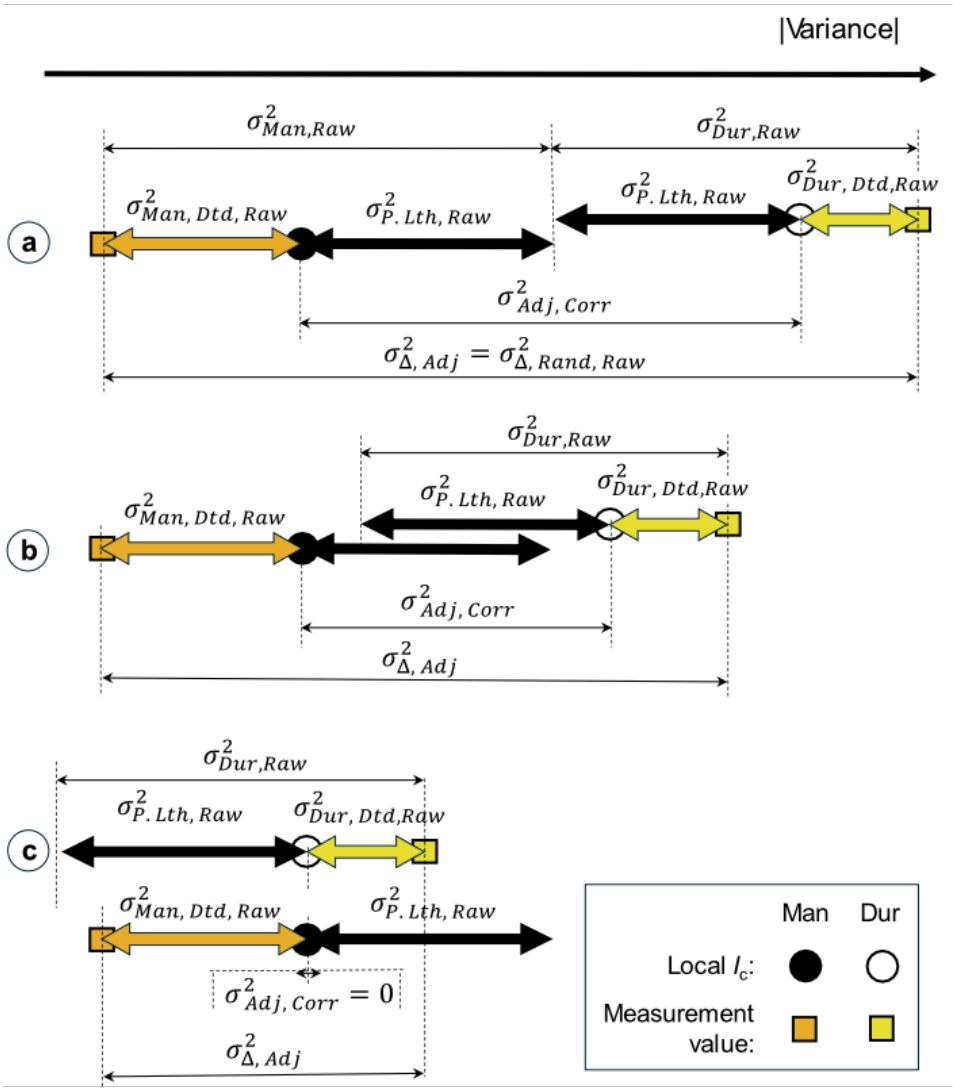

Figure 5: The sum of the (normalised) variances rule: The variance of the difference between the data (properties) on adjacent strands from Durham and the manufacturer $\sigma^2_{\Delta,\,Adj}$ ($\sigma^2_{Adj,\,Corr}$) is denoted by the separation of the two squares (circles). In ⓐ adjacent strands are as uncorrelated as the piece-length ends, ⓑ they are partially correlated, and in ⓒ they are perfectly correlated (i.e. $\sigma^2_{Adj,\,Corr} = 0$,) respectively. $\sigma^2_{Dur,\,Raw}$, $\sigma^2_{P.Lth,\,Raw}$ and $\sigma^2_{Dur,\,Dtd,\,Raw}$ are the variances of the data in Durham (and similarly for the manufacturer with subscript Man), the piece-length ends, and that introduced by the laboratory from door-to-data (i.e. processing-and-measurement). This figure considers raw data, but equally well applies to smoothed data.

.

Table 5: Analysis of all measurements on the Internal Tin (IT) Nb_3Sn strand. The abbreviations used are I_c: critical current; n-value: index of transition; RRR: residual resistivity ratio; Q: hysteretic losses; CnC ratio: copper to non-copper ratio; HT: heat-treatment; Temp.: temperature control; PSS: physical strand size; IR: image resolution. The smoothed data (subscript: Smd) were obtained after subtracting a 20-point moving average from the raw data (subscript: Raw). The variables used are defined in Section 7.1. The dashes denote non-physical (negative variance) values.

		I_c at 12.0 T		n-value		RRR		Q		CnC ratio		Strand diameter		Twist pitch		Plating thickness	
Units		A		Dimensionless		Dimensionless		mJ cm^{-3}		Dimensionless		mm		mm		µm	
Estimated random [systematic] error.		1.5%, [1.5%]		2%, [1.5%]		2%, [1%]		2%, [2%]		1%, [1%]		0.1%, [0.1%]		8%, [1%]		0.2%, [0.15%]	
Dominated by		HT		HT		Temp.		HT + PSS		IR		Instr. Spec.		Angle		Strand dia.	
Laboratory		Dur	Man	Dur	Man	Dur	Man	Dur	Man	Dur	Man	Dur	Man	Dur	Man	Dur	Man
		Internal Tin Nb_3Sn															
Strand number:	Both labs, [Dur]	980, [1065]		977, [1065]		1323, [1725]		373, [488]		907, [973]		797, [963]		900, [963]		905, [965]	
$\bar{x}_{Lab}$	(Various)	275.7	282.4	36.1	39.1	143.7	160.0	278	255	1.008	0.993	0.823 15	0.821 69	14.33	15.73	1.221	1.304
$\Delta\bar{x}$	(%)	−2.4		−8.5		−11.4		8.1		1.5		0.18		−9.8		−6.8	
$\tilde{\sigma}_{Lab,\,Raw}$	(%)	6.2	5.3	13.0	15.9	22.4	21.9	13.2	17.5	5.8	5.4	0.15	0.13	5.2	5.9	10.8	13.2
$\tilde{\sigma}_{\Delta,\,Adj}$, $[\tilde{\sigma}_{\Delta,\,Rand,\,Raw}]$	(%)	4.1, [8.2]		15.5, [20.5]		25.1, [31.4]		21.3, [21.9]		6.0, [8.0]		0.12, [0.20]		7.5, [7.8]		10.9, [17.0]	
$\tilde{\sigma}_{Lab,\,Dtd,\,Raw}$	Max (%)	3.7	1.8	8.8	12.7	18.1	17.4	12.7	17.1	4.5	4.0	0.10	0.07	4.9	5.7	5.5	9.4
	Min (%)	3.5	1.5	2.0	9.4	5.1	2.0	2.0	11.7	2.3	1.0	0.07	0.07	4.9	5.7	0.1	7.6
$\tilde{\sigma}_{P.\,Lth,\,Raw}$	Max (%)	5.1		12.8		21.8		13.0		5.3		0.11		1.7		10.8	
	Min (%)	5.0		9.5		13.3		3.7		3.7		0.11		1.7		9.3	
		Smoothed analysis after 20-point moving average subtracted															
$\tilde{\sigma}_{Lab,\,Smd}$	(%)	3.7	4.0	8.4	13.9	18.5	20.9	12.2	12.5	5.4	5.0	0.12	0.11	4.7	5.3	6.7	7.5
$\tilde{\sigma}_{\Delta\,Adj}$, $[\tilde{\sigma}_{\Delta,\,Rand,\,Smd}]$	(%)	4.1, [5.4]		15.5, [16.3]		25.1, [27.6]		21.3, [17.5]		6.0, [7.4]		0.12, [0.17]		7.5, [7.1]		10.9, [10.0]	
$\tilde{\sigma}_{Lab,\,Dtd,\,Smd}$	Max (%)	2.7	3.1	7.7	13.5	16.4	19.0	-	-	4.5	4.0	0.09	0.08	-	-	-	-
	Min (%)	1.5	2.1	2.0	11.3	2.0	9.9	-	-	2.3	1.0	0.09	0.08	-	-	-	-
$\tilde{\sigma}_{P.\,Lth,\,Smd}$, $[\tilde{\sigma}_{MA}]$	Max (%)	3.4,	[4.3]	8.2,	[8.8]	18.4,	[11.4]	- ,	[8.9]	4.9,	[2.1]	0.08,	[0.08]	- ,	[2.3]	- ,	[9.6]
	Min (%)	2.5,		3.4,		8.6,		- ,		3.0,		0.08,		- ,		- ,	

Table 6: Bronze Route (BR) Nb_3Sn strand measurements and analysis. The abbreviations used are I_c: critical current; n-value: index of transition; RRR: residual resistivity ratio; Q: hysteretic losses; CnC ratio: copper to non-copper ratio; HT: heat-treatment; Temp.: temperature control; PSS: physical strand size; IR: image resolution. The smoothed data (subscript: Smd) were obtained after subtracting a 20-point moving average from the raw data (subscript: Raw). The variables used are defined in Section 7.1. The dashes denote non-physical (negative variance) values.

		I_c at 12.0 T		n-value		RRR		Q		CnC ratio		Strand diameter		Twist pitch		Plating thickness	
	Units	A		Dimensionless		Dimensionless		mJ cm^{-3}		Dimensionless		mm		mm		µm	
Estimated random [systematic] error.		1.5%, [1.5%]		2%, [1.5%]		2%, [1%]		2%, [2%]		1%, [1%]		0.1%, [0.1%]		8%, [1%]		0.2%, [0.15%]	
Dominated by		HT		HT		Temp.		HT + PSS		IR		Instr. Spec.		Angle		Strand dia.	
Laboratory		Dur	Man	Dur	Man	Dur	Man	Dur	Man	Dur	Man	Dur	Man	Dur	Man	Dur	Man
		Bronze Route Nb_3Sn															
Strand number:	Both labs, [Dur]	396, [409]		396, [409]		464, [490]		170, [179]		342, [354]		342, [354]		[365]		[342]	
$\bar{x}_{Lab}$	(Various)	197.4	199.4	43.0	43.9	106.5	115.2	59	66	0.931	0.936	0.820 49	0.820 55	15.56	n/a	1.31	n/a
$\Delta\bar{x}$	(%)	−1.0		−2.3		−8.2		−12.7		−0.5		−0.01		n/a		n/a	
$\tilde{\sigma}_{Lab,\,Raw}$	(%)	2.1	2.0	3.3	4.2	11.0	10.8	21.1	26.3	2.1	2.6	0.15	0.15	6.9	n/a	14.7	n/a
$\tilde{\sigma}_{\Delta,\,Adj}$, $[\tilde{\sigma}_{\Delta,\,Rand,\,Raw}]$	(%)	1.2, [2.9]		3.6, [5.3]		6.3, [15.4]		10.0, [31.2]		2.3, [3.4]		0.08, [0.21]		n/a , [n/a]		n/a , [n/a]	
$\tilde{\sigma}_{Lab,\,Dtd,\,Raw}$	Max (%)	1.0	0.7	1.8	3.1	4.7	4.2	-	-	1.2	2.0	0.06	0.06	n/a	n/a	n/a	n/a
	Min (%)	1.0	0.7	1.8	3.1	2.9	2.0	-	-	1.0	1.8	0.06	0.06	6.9	n/a	0.2	n/a
$\tilde{\sigma}_{P.\,Lth,\,Raw}$	Max (%)	1.9		2.8		10.6		-		1.8		0.11		0		14.7	
	Min (%)	1.9		2.8		9.9		-		1.7		0.14		n/a		n/a	
		Smoothed analysis after 20-point moving average subtracted															
$\tilde{\sigma}_{Lab,\,Smd}$	(%)	1.6	1.5	2.9	2.8	7.9	7.8	13.8	15.9	2.1	2.3	0.12	0.11	4.9	n/a	10.4	n/a
$\tilde{\sigma}_{\Delta\,Adj}$, $[\tilde{\sigma}_{\Delta,\,Rand,\,Smd}]$	(%)	1.2, [2.2]		3.6, [4.1]		6.3, [11.1]		10.0, [17.6]		2.3, [3.1]		0.08, [0.16]		n/a , [n/a]		n/a , [n/a]	
$\tilde{\sigma}_{Lab,\,Dtd,\,Smd}$	Max (%)	0.9	0.8	2.6	2.5	4.5	4.4	4.3	9.0	1.5	1.8	0.07	0.05	n/a	n/a	n/a	n/a
	Min (%)	0.9	0.8	2.0	1.9	2.0	1.6	2.0	8.1	1.0	1.4	0.07	0.05	4.9	n/a	0.2	n/a
$\tilde{\sigma}_{P.\,Lth,\,Smd}$, $[\tilde{\sigma}_{MA}]$	Max (%)	1.3,	[1.2]	2.1,	[2.3]	7.6,	[7.1]	13.7,	[17.5]	1.8,	[0.9]	0.07,	[0.09]	0 ,	[4.7]	10.4,	[9.9]
	Min (%)	1.3,		1.3,		6.5,		13.1,		1.5,		0.07,		n/a ,		n/a ,	

Table 7: Nb-Ti strand measurements and analysis. The abbreviations used are I_c: critical current; n-value: index of transition; RRR: residual resistivity ratio; Q: hysteretic losses; CnC ratio: copper to non-copper ratio; PSS: physical strand size. The smoothed data (subscript: Smd) were obtained after subtracting a 20-point moving average from the raw data (subscript: Raw). The variables used are defined in Section 7.1. The dashes denote non-physical (negative variance) values.

		I_c at 6.4 T		n-value		RRR		Q		CnC ratio		Strand diameter		Twist pitch		Plating thickness	
Units		A		Dimensionless		Dimensionless		mJ cm^{-3}		Dimensionless		mm		mm		µm	
Estimated random [systematic] error.		1%, [0.5%]		1.5%, [0.5%]		1%, [1%]		0.5%, [2%]		0.1%, [0.1%]		0.1%, [0.1%]		8%, [1%]		0.3%, [0.3%]	
Dominated by		Non-power law		Non-power law		Temp.		PSS		Instr. Spec.		Instr. Spec.		Angle		Strand dia.	
Laboratory		Dur	Man	Dur	Man	Dur	Man	Dur	Man	Dur	Man	Dur	Man	Dur	Man	Dur	Man
		Nb–Ti															
Strand number:	Both labs, [Dur]	174, [320]		174, [320]		106, [320]		69, [320]		115, [323]		174, [320]		116, [320]		166, [320]	
$\bar{x}_{Lab}$	(Various)	336.6	328.1	38.6	41.2	130	134	46.4	44.7	1.596	1.626	0.7323	0.7322	15.23	15.14	1.61	1.66
$\Delta\bar{x}$	(%)	2.5		−6.6		−2.9		3.8		−1.9		0.02		0.6		−2.7	
$\tilde{\sigma}_{Lab,\,Raw}$	(%)	2.2	2.1	4.4	8.7	11.0	10.4	3.9	4.0	2.9	2.6	0.20	0.16	5.8	4.1	11.2	7.9
$\tilde{\sigma}_{\Delta,\,Adj}$, $[\tilde{\sigma}_{\Delta,\,Rand,\,Raw}]$	(%)	1.7, [3.0]		9.3, [9.7]		8.8, [15.0]		4.4, [5.6]		3.1, [3.9]		0.23, [0.25]		6.7, [7.0]		7.0, [13.7]	
$\tilde{\sigma}_{Lab,\,Dtd,\,Raw}$	Max (%)	1.3	1.1	3.9	8.5	6.7	5.7	3.0	3.2	2.4	2.0	0.18	0.14	5.6	3.7	-	-
	Min (%)	1.0	0.8	1.5	7.7	3.7	1.0	0.5	1.0	1.3	0.1	0.16	0.10	5.6	3.7	-	-
$\tilde{\sigma}_{P.\,Lth,\,Raw}$	Max (%)	2.0		4.1		10.4		3.9		2.6		0.12		1.7		-	
	Min (%)	1.8		2.1		8.7		2.4		1.7		0.08		1.7		-	
		Smoothed analysis after 20-point moving average subtracted															
$\tilde{\sigma}_{Lab,\,Smd}$	(%)	1.7	1.6	4.1	8.0	9.8	9.0	3.0	3.2	2.4	2.1	0.18	0.15	5.5	4.1	7.1	4.5
$\tilde{\sigma}_{\Delta\,Adj}$, $[\tilde{\sigma}_{\Delta,\,Rand,\,Smd}]$	(%)	1.7, [2.3]		9.3, [8.9]		8.8, [13.2]		4.4, [4.4]		3.1, [3.1]		0.23, [0.23]		6.7, [6.9]		7.0, [8.4]	
$\tilde{\sigma}_{Lab,\,Dtd,\,Smd}$	Max (%)	1.3	1.1	-	-	6.8	5.6	-	-	2.3	2.0	0.18	0.15	5.4	4.0	6.3	3.1
	Min (%)	1.0	0.8	-	-	4.0	1.0	-	-	1.2	0.1	0.14	0.10	5.4	4.0	5.5	0.3
$\tilde{\sigma}_{P.\,Lth,\,Smd}$, $[\tilde{\sigma}_{MA}]$	Max (%)	1.4,	[1.3]	- ,	[2.7]	8.9,	[4.7]	- ,	[2.1]	2.1,	[1.5]	0.11,	[0.06]	1.0,	[1.2]	4.5,	[7.5]
	Min (%)	1.1,		- ,		7.1,		- ,		0.5,		0.03,		1.0,		3.3,	

However, an example of the central experimental result in this paper is that the experimental value for the variance of the difference in I_c, between the Durham data and that of the manufacturer for the adjacent strands, is significantly lower than the value derived for randomised pairs since $\tilde{\sigma}_{\Delta,\,Adj} = 4.1\,\%$ and $\tilde{\sigma}_{\Delta,\,Rand,\,Raw} = 8.2\,\%$. These lower experimental values are found in all the measurements in Tables 5 to 7. It is this difference and consequential positive correlation between the adjacent strands, that provides the additional information that will enable us to find (and constrain) the limits for the lab errors and strand variability.

7.2 Maximum and minimum values derived from adjacent strand measurements

Rearranging Eqns. 6, 7 and 8, we can find the separate contributions from each of the laboratories and the strands themselves that we are most interested in (i.e. $\tilde{\sigma}_{Dur,\,Dtd,\,Raw}$, $\tilde{\sigma}_{Man,\,Dtd,\,Raw}$ and $\tilde{\sigma}_{P.Lth,\,Raw}$), in terms of the measured parameters $\tilde{\sigma}_{\Delta,\,Adj,\,Raw}$, $\tilde{\sigma}_{Dur,\,Raw}$ and $\tilde{\sigma}_{Man,\,Raw}$, and the variable that describes the degree of correlation between adjacent strands $\tilde{\sigma}_{Adj,\,Corr}$, where,

$$\tilde{\sigma}^2_{Dur,\,Dtd,\,Raw} = \frac{1}{2}\left\{(\tilde{\sigma}^2_{\Delta,\,Adj} - \tilde{\sigma}^2_{Adj,\,Corr}) + \tilde{\sigma}^2_{Dur,Raw} - \tilde{\sigma}^2_{Man,Raw}\right\}, \tag{10}$$

the equivalent equation for the manufacturer's laboratory is

$$\tilde{\sigma}^2_{Man,\,Dtd,\,Raw} = \frac{1}{2}\left\{(\tilde{\sigma}^2_{\Delta,\,Adj} - \tilde{\sigma}^2_{Adj,\,Corr}) - \tilde{\sigma}^2_{Dur,\,Raw} + \tilde{\sigma}^2_{Man,\,Raw}\right\}, \tag{11}$$

and the variance for the ends of the piece-lengths is

$$\tilde{\sigma}^2_{P.Lth,\,Raw} = \frac{1}{2}\left\{-(\tilde{\sigma}^2_{\Delta,\,Adj} - \tilde{\sigma}^2_{Adj,\,Corr}) + \tilde{\sigma}^2_{Dur,\,Raw} + \tilde{\sigma}^2_{Man,\,Raw}\right\}. \tag{12}$$

Since the degree of correlation between adjacent strands (i.e. $\tilde{\sigma}^2_{Adj,\,Corr}$) is *a priori* not known, we consider in turn the two extreme limits of perfectly correlated and maximum uncorrelated adjacent strands to calculate the allowed range for these variables.

7.2.1 Identical adjacent strands. In the limiting case where adjacent strands approach being identical (i.e. the repeat measurement limit),

$$\tilde{\sigma}^2_{Adj,\,Corr} \geq 0\,. \tag{13}$$

Substituting Eq. 13 into Eqs. 10 to 12 leads to the maximum (upper bound) values for Durham

$$\tilde{\sigma}^2_{Dur,\,Dtd,\,Raw} \leq \frac{1}{2}\left(\tilde{\sigma}^2_{\Delta,\,Adj} + \tilde{\sigma}^2_{Dur,Raw} - \tilde{\sigma}^2_{Man,Raw}\right), \tag{14}$$

and the equivalent equation for the manufacturer's laboratory,

$$\tilde{\sigma}^2_{Man,\,Dtd,\,Raw} \leq \frac{1}{2}\left(\tilde{\sigma}^2_{\Delta,\,Adj} - \tilde{\sigma}^2_{Dur,\,Raw} + \tilde{\sigma}^2_{Man,\,Raw}\right). \tag{15}$$

We also have the variance for piece-length ends themselves, which is a minimum (lower bound) given by

$$\tilde{\sigma}^2_{P.Lth,\,Raw} \geq \frac{1}{2}\left(-\tilde{\sigma}^2_{\Delta,\,Adj} + \tilde{\sigma}^2_{Dur,\,Raw} + \tilde{\sigma}^2_{Man,\,Raw}\right) . \tag{16}$$

We can rewrite these three equations in terms of their limiting values, and in a form using Bienayme's identity (Eq. 9) that makes explicit the additional information that measurements on adjacent strands bring:

$$\tilde{\sigma}^2_{Dur,\,Dtd,\,Raw}(Max) = \tilde{\sigma}^2_{Dur,Raw} - \frac{1}{2}(\tilde{\sigma}^2_{\Delta,\,Rand,\,Raw} - \tilde{\sigma}^2_{\Delta,\,Adj}) , \tag{17}$$

$$\tilde{\sigma}^2_{Man,\,Dtd,\,Raw}(Max) = \tilde{\sigma}^2_{Man,Raw} - \frac{1}{2}(\tilde{\sigma}^2_{\Delta,\,Rand,\,Raw} - \tilde{\sigma}^2_{\Delta,\,Adj}) , \tag{18}$$

and

$$\tilde{\sigma}^2_{P.Lth,\,Raw}(Min) = \frac{1}{2}(\tilde{\sigma}^2_{\Delta,\,Rand,\,Raw} - \tilde{\sigma}^2_{\Delta,\,Adj}) . \tag{19}$$

Were there no measurements from adjacent strands, we would set the terms in round brackets to zero and recover the standard limits for single lab measurements. As shown in Table 4, the raw data from Durham has $\tilde{\sigma}^2_{Dur,\,Raw} = 6.2\,\%$ and from the manufacturer has 5.3 %. However, because of the adjacent strand measurements, the lab errors are very significantly smaller $\tilde{\sigma}_{Dur,\,Dtd,\,Raw}(\mathrm{Max}) = 3.7\,\%$ and $\tilde{\sigma}_{Man,\,Dtd,\,Raw}(\mathrm{Max}) = 1.8\,\%$, which brings them much closer to the estimated lower bound value (1.5 %). Similarly, the strands' variability is markedly increased from zero (for a single lab with no repeat measurements) to $\tilde{\sigma}_{P.Lth,\,Raw}(Min) = 5.0\,\%$.

7.2.2 Weakly correlated adjacent strands. We now consider the opposite limit that follows from considering the maximum value of $\tilde{\sigma}_{Adj,\,Corr}$ that still provides physical solutions. Given Eq. 13 we could consider $\tilde{\sigma}^2_{Adj,\,Corr} \leq 2\tilde{\sigma}^2_{P.Lth,\,Raw}$ or perhaps that all the variances must be positive definite. However, we make the more restrictive constraint that the random lab errors in Durham must be at least those random errors estimated for 'door-to-data' by Durham scientists (i.e. $\tilde{\sigma}_{Est,\,Rand}$). We also make the working assumption that the estimated Durham random lab errors provide a lower bound for the manufacturer as well, which given Eqs. 6 and 7 requires, in practice, that the lab whose data has the lowest variance, has at least those random errors estimated in Durham. If, for a particular measurement, the Durham lab data has the lowest variance, the lower bound condition is

$$\tilde{\sigma}^2_{Dur,\,Dtd,\,Raw} \;\geq \tilde{\sigma}^2_{Est,\,Rand} . \tag{20}$$

This inequality is complementary to Eq. 10. In terms of its limiting value, this equation is rewritten

$$\tilde{\sigma}^2_{Dur,\,Dtd,\,Raw}(Min) \;= \tilde{\sigma}^2_{Est,\,Rand} . \tag{21}$$

Substituting Eq. 20 into Eq. 10 gives the constraint

$$\tilde{\sigma}^2_{Adj,\,Corr} \leq \tilde{\sigma}^2_{\Delta,\,Adj} + \tilde{\sigma}^2_{Dur,Raw} - \tilde{\sigma}^2_{Man,Raw} - 2\tilde{\sigma}^2_{Est,\,Rand}\,, \tag{22}$$

which provides a maximum value for the correlation between adjacent strands. This can be rewritten in the form

$$\tilde{\sigma}^2_{Adj,\,Corr} \leq 2\,(\tilde{\sigma}^2_{Dur,Raw} - \tilde{\sigma}^2_{Est,\,Rand}) - (\tilde{\sigma}^2_{\Delta,\,Rand,\,Raw} - \tilde{\sigma}^2_{\Delta,\,Adj})\,, \tag{23}$$

which explicitly shows that when the adjacent strands are as uncorrelated as randomly chosen piece-length ends (i.e. $\tilde{\sigma}^2_{\Delta,\,Adj} = \tilde{\sigma}^2_{\Delta,\,Rand,\,Raw}$), the single lab result with no repeat measurements is again recovered. Substituting Eq. 22 into Eqs. 11 and 12 gives the remaining two limits

$$\tilde{\sigma}^2_{Man,\,Dtd,\,Raw}(Min) = \tilde{\sigma}^2_{Man,\,Raw} - \tilde{\sigma}^2_{Dur,\,Raw} + \tilde{\sigma}^2_{Est,\,Rand}\,, \tag{24}$$

and

$$\tilde{\sigma}^2_{P.Lth,\,Raw}(Max) = \tilde{\sigma}^2_{Dur,\,Raw} - \tilde{\sigma}^2_{Est,\,Rand}\,. \tag{25}$$

To derive the equivalent equations when the manufacturer's estimates more tightly constrain the data, we replace the estimates from the Durham lab by those from the manufacturer and rotate Dur and Man in Eqs 20 to 25. In practice, we calculate these parameters by increasing $\tilde{\sigma}^2_{Adj,\,Corr}$ until the variance of the "door to data" of one or other of the labs reaches their estimated value. In Table 4, we have calculated the limiting values using Eqs. 21, 24 and 25. We note that these equations can be obtained more directly by substituting Eq. 20 directly into Eq. 6. Using the raw data, we find for the two laboratories that the minimum random errors from the raw data are $\tilde{\sigma}_{Dur,\,Dtd,\,Raw}(\mathrm{Min}) = 3.5\,\%$ and $\tilde{\sigma}_{Man,\,Dtd,\,Raw}(\mathrm{Min}) = 1.5\,\%$, and the maximum piece-length end variability is $\tilde{\sigma}_{P.Lth,\,Raw}(\mathrm{Max}) = 5.1\,\%$.

7.3 Systematic differences and identifying long-term drift

The data in Figure 3 show that we can consider the variations in Durham's and the manufacturer's data in three categories: First there is the systematic difference between the average values. This difference may be attributed to, say, inaccuracies in the calibration of instruments, or systematic differences in the handling of the brittle Nb_3Sn, or gas purity differences in the heat-treatments between the two labs. The second category is the long-term drift, clearly seen in both (independent) datasets, that we associate with variations in the manufacturing process, such as wear on the drawing dies. It is shown by the black line in Figure 3 ⓑ. We note that measurements from several labs measuring adjacent strands would enable more accurate identification of long-term drifts from each of the partner labs and the manufacturing, and that we would not expect these long-term drifts to obey normal statistics. The third category includes both the scatter in the data that occurs from short-length variations in manufacture manifest at the ends

of the piece-lengths (say variations in raw material purity or hardness), as well as the errors introduced by the laboratories themselves during processing-and-measurement.

Figure 3 shows our approach to removing the long-term drift. We first subtract the difference in the averages $\Delta\bar{x}_{Lab}$ between both laboratories and then apply a Savitzky-Golay moving average (MA) smoothing procedure to the total of both datasets [48]. We have chosen the number of points in the window to be ~ 20, as have other authors [4], and show below that the parameters of interest and the conclusions of this work are broadly insensitive to this choice of window size. The data in Figure 3 ⓒ shows the data from both laboratories after it has been smoothed. These data are replotted on the RHS of Figure 4 and provides the NSD for the smoothed data from each of the laboratories (i.e. $\tilde{\sigma}_{(Dur,\,Smd)}$ and $\tilde{\sigma}_{(Man,\,Smd)}$). After the long-term drift has been removed, as expected, both the maximum and minimum limiting values for the NSD of the strand variability decreases for all measurements (cf. Tables 5 to 7). For the IT I_c measurements, the range for $\tilde{\sigma}_{P.Lth,\,Raw}$ is 5.0 % to 5.1 % whereas after 20-point smoothing, the limiting values decrease to give a range of 2.5 % to 3.4 %.

7.4 Analysis of smoothed data

Just as we applied Eqns. 10 to 12 to the raw data, we can equally apply them to the data after smoothing (i.e. replace the subscript Raw in them by Smoothed (Smd)). Table 4 provides the variables calculated after smoothing for the random lab errors (i.e. $\tilde{\sigma}_{Dur,\,Dtd,\,Smd}$ and $\tilde{\sigma}_{Man,\,Dtd,\,Smd}$) and the strand variability ($\tilde{\sigma}_{P.Lth,\,Smd}$). Table 4 gives the maximum and minimum Durham lab errors as 2.7 % and 1.5 %, and those for the manufacturer as 3.1 % and 2.1 %. Similarly, the maximum and minimum values for the strand variability are 3.4 % and 2.5 %. Although the long-term drift (or moving average) does not obey normal statistics, we usefully characterise the degree of smoothing with a NSD of 4.3 %. Also we note the variable $\tilde{\sigma}_{\Delta,\,Adj}$ (4.1 %) is independent of whether smoothing is done or not, and $\tilde{\sigma}_{\Delta,\,Rand,\,Smd}$ is 5.4 %.

7.5 Window size independence

The data in Figure 6 and Table 4 shows how the important physical parameters for the IT I_c measurements vary as a function of window size and can be used to justify the window size of 20. At large window sizes of ~ 80, these parameters asymptotically saturate, consistent with smoothing out long-term variations as required. Table 4 demonstrates that the variances of the smoothed data systematically decrease as the window size decreases. However, if the window size gets too small, it starts over-smoothing the data and we get non-physical results: some of the short-term lab variations and $\tilde{\sigma}_{P.Lth,Smd}$ artificially drop to zero, and the adjacent strands become negatively (non-physically) correlated, evidenced by $\tilde{\sigma}_{\Delta,Adj} > \tilde{\sigma}_{\Delta,Rand,Smd}$ (i.e. 15.5 % > 15.4 % in Table 4). However, in the intermediate range of window sizes from 20 to 80, for both the maximum and minimum limits, to a good approximation we find that,

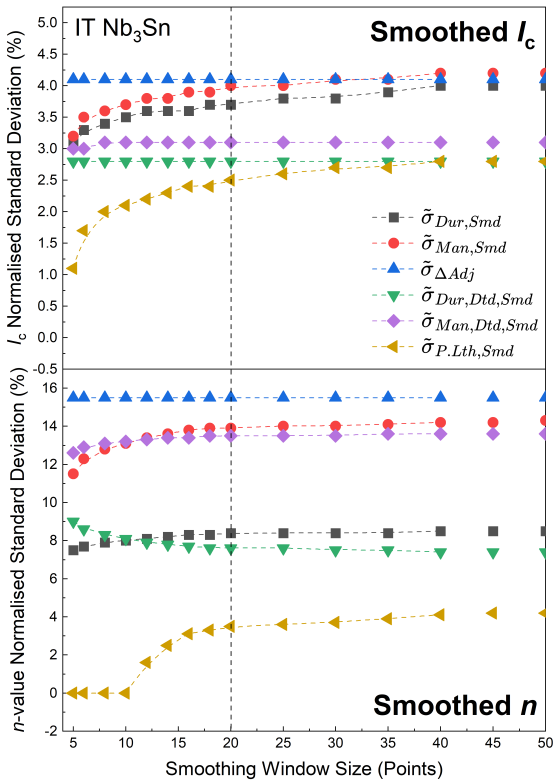

Figure 6: Statistical parameters (normalised standard deviation) derived from smoothed data, as a function of smoothing window size for internal tin (IT Nb_3Sn). ⓐ I_c data. ⓑ n-value data. The vertical dashed line shows the 20-point window size chosen for the moving average in this work.

$$\tilde{\sigma}^2_{P.Lth,Raw} \approx \tilde{\sigma}^2_{P.Lth,\,Smd}(Window\ size) + \tilde{\sigma}^2_{MA}(Window\ size)\,, \tag{26}$$

where $\tilde{\sigma}^2_{P.Lth,Raw}$ is very weakly dependent on window size as shown in Table 6. Equation 26 is consistent with the total piece-length variance being broadly independent of how we choose to assign the component short-term and long-term scale variances. Equally, the limiting values for $\tilde{\sigma}_{Dur,\,Dtd,\,Smd}$ and $\tilde{\sigma}_{Man,\,Dtd,\,Smd}$ are also broadly independent of window size, consistent with correctly assigning these values to the uncertainties associated with the laboratories alone.

The different distributions underpinning the analysis in this section are shown in Figure 7: the distribution characterised by taking the raw data from the two laboratories and considering all possible pairing gives $\tilde{\sigma}_{\Delta,\,Rand,\,Raw} = 8.2\,\%$. After smoothing the datasets from both labs, the random distribution narrows because the moving average smoothing maps to those measurements from the two laboratories that are positively correlated and $\tilde{\sigma}_{\Delta,\,Rand,\,Smd} = 5.4\,\%$. Nevertheless, in the third distribution the experimental data remains the narrowest, even after smoothing (where $\tilde{\sigma}_{\Delta,\,Adj} = 4.1\,\%$), demonstrating that the adjacent strands are positively correlated and providing the key additional information used in this analysis.

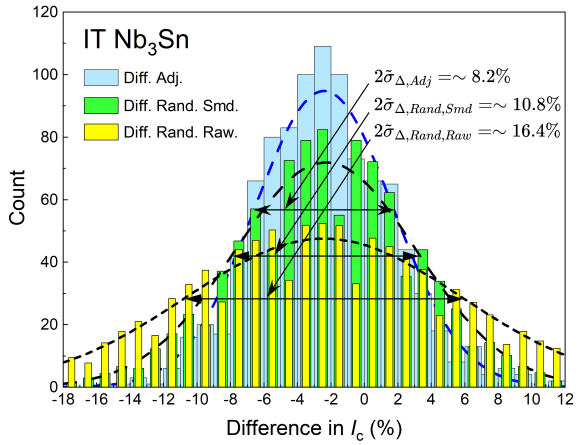

Figure 7: I_c distributions for the differences between the Durham and manufacturer adjacent pairs of internal tin (IT Nb_3Sn) strands. Shown are: the experimental differences distribution ($\tilde{\sigma}_{\Delta,\,Adj}$); the differences between the distribution of randomly paired smoothed data from Durham and the manufacturer ($\tilde{\sigma}_{\Delta,\,Rand,\,Smd}$); and the differences between the distribution of randomly paired raw measurements from Durham and the manufacturer ($\tilde{\sigma}_{\Delta,\,Rand,\,Raw}$). The best-fit normal distributions are shown by the black dashed lines.

7.6 Statistical analysis of the IT Nb_3Sn n-values

Table 4, and Figures 6 and 8 show the analysis of the IT Nb_3Sn n-value data. Similarly to the IT I_c data, we again find: a moving average in the data from both labs that we can associate with variations in the long-term drift of the strand properties; after the MA has been subtracted, the correlation between the adjacent strands is weaker as demonstrated by the high n-value strands in the smoothed Durham data being quite evenly spread across the manufacturers' distribution (cf. Figure 3) and evidenced by the experimental data for the NSD of the difference between n-values of adjacent strands ($\tilde{\sigma}_{\Delta,\,Adj} = 15.5\,\%$) being similar to randomly chosen pairs ($\tilde{\sigma}_{\Delta,\,Adj} = 16.2\,\%$).

7.7 Losses, Q - an outlier

Throughout this paper we have calculated the various values of $\tilde{\sigma}$ from the relevant distribution of experimental data directly using the definition of the standard deviation. The error bars for these values can be estimated using the $1/\sqrt{n}$ law, which typically gives 2 - 10 % and have been confirmed by fitting the various distributions using a commercial package. The data for the IT Q loss data are an outlier in this work as shown in Figure 9. They do not obey a normal distribution and the error bars are commensurately larger. The manufacturer's data show two distinct populations, that we associate most probably with handling.

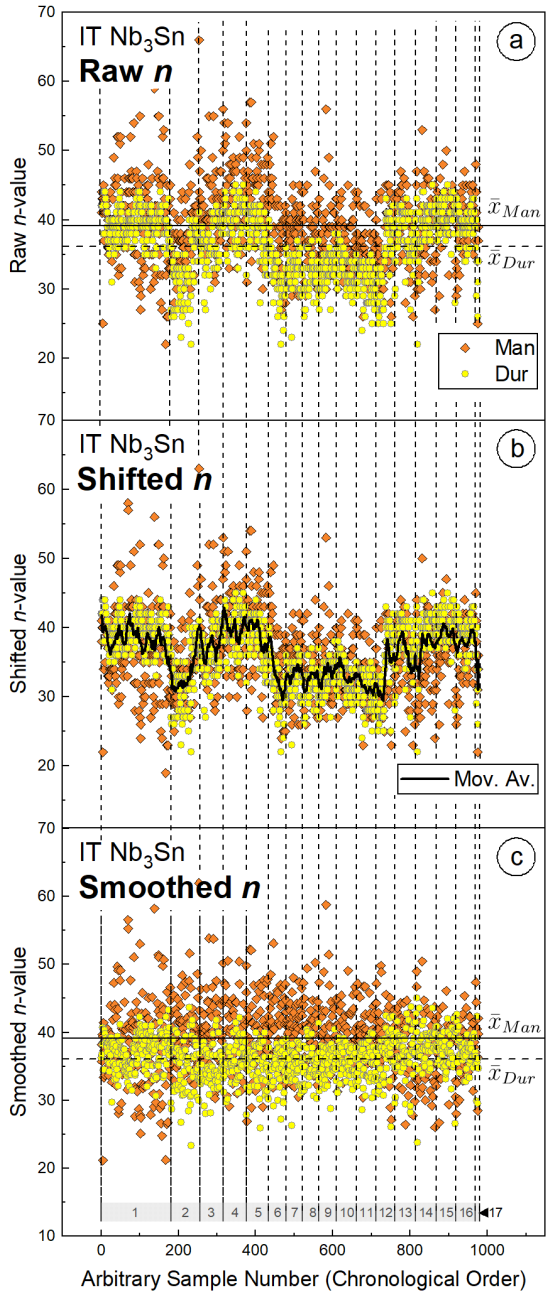

Figure 8: The Durham (Dur) and manufacturer (Man) n-value data for the internal tin (IT Nb_3Sn) strands in chronological order. ⓐ Raw data, ⓑ a 20-point moving average (MA) of the Durham data and the manufacturer data after the latter has been shifted to the Durham mean and ⓒ the smoothed data for both labs after subtracting the MA from the raw data and the mean of the manufacturer data has been restored. The strands received by Durham were grouped into 17 individual deliverables represented here by vertical dashed lines.

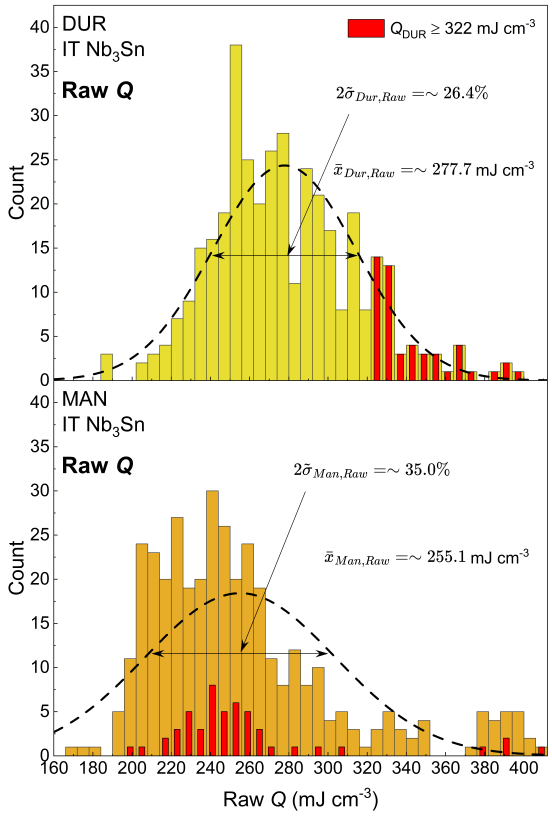

Figure 9: The normal distributions (black dashed lines) for the ⓐ Durham and ⓑ manufacturer bronze route (BR Nb_3Sn) raw hysteresis loss (Q) data. The red bars identify those Durham strands with high n-values 's, together with their associated adjacent strand data from the manufacturer.

8 Statistical analysis of the BR Nb_3Sn I_c and n-value data

The vast majority of the experimental work is related to the I_c and n-values of the two Nb_3Sn strands. Following the detailed IT data and analysis, we briefly present the equivalent BR Nb_3Sn data in Figures 10 and Figure 11 . Figure 10 again shows the moving average that is common to the data sets in both laboratories. After it has been subtracted, there remains a significant positive correlation between the adjacent strands as was found for the IT strands. The measured maximum lab errors were below the estimated minimum values, so to within the accuracy of this particular measurement, we conclude there are no significant differences between the properties of the adjacent strands and reset the estimated minimum values to be identical to the measured maximum values in Table 6. We find that the Durham lab error was ∼1.8 %, that for the manufacturer was ∼3.1 % and the (short time-scale) piece-length ends variability was ∼ 2.8 %. We conclude that for these measurements on this BR strand, strand handling and gas purity during processing played no significant role. For the BR Nb_3Sn n-value data, Figure 11 shows the result of subtracting the moving average from the raw data.

There is a general upwards drift over the course of the campaign, showing the limitations of characterising the moving average with a normalised standard deviation (i.e. $\tilde{\sigma}_{MA}$ = 1.2 %). Nevertheless, the measurements are all normal distributions and are well characterised with no evidence for any significant unidentified sources of error (i.e. the maximum and minimum values for both the random errors from the laboratories and the variability of the piece-lengths are similar).

9 Categorising the data.

In this section, we consider three ratios that help categorise and set the broad canvas for the large datasets in Tables 5 - 7. We use the notation $\tilde{\sigma}_{Lab,\,Dtd,\,Smd\,or\,Raw}$ which means smoothed values $\tilde{\sigma}_{Lab,\,Dtd,\,Smd}$ when available, and the raw data $\tilde{\sigma}_{Lab,\,Dtd,\,Raw}$ for those remaining five measurements where there are dashes for the smoothed data in Tables 5 - 7.

9.1 The range of the random lab errors.

First, we address the range of the random lab error for a specific measurement given by the ratio of the maximum lab error divided by its minimum (i.e. $\tilde{\sigma}_{Lab,\,Dtd,\,Smd\,or\,Raw}(\mathrm{Max})/\tilde{\sigma}_{Lab,\,Dtd,\,Smd\,or\,Raw}(\mathrm{Min})$). We (arbitrarily) consider the measurements in four different types, which establishes the concept of well (or poorly) characterised measurements where the random lab errors are well known:

i) Very well characterised measurements [IT(Strand diameter and Twist pitch), BR(I_c and strand diameter) and Nb–Ti(Twist pitch)]: These five datasets are identified by the smoothed or raw maximum lab error for one or other of the labs (e.g. $\tilde{\sigma}_{Lab,\,Dtd,\,Smd\,or\,Raw}(\mathrm{Max})$)) being less than or equal to the estimated error with the result that we have reset the estimated minimum value to equal the maximum lab error and the range of the lab errors to be 1. In these cases, as with repeat measurements, to within the accuracy of the measurements, the properties of the adjacent strands are identical (i.e. $\tilde{\sigma}_{Adj,\,Corr} = 0$ as shown in Figure 5), the errors introduced by each of the two labs can be completely separated (deconvoluted) from the variability in manufacture of the strands, and we conclude there are no unaccounted for random errors (e.g. heat-treatment or handling errors).

ii) Well characterised random lab errors [IT(I_c), BR(n-value, Q and CnC ratio) and Nb–Ti(I_c)]: These five measurements have low ratios between 1.0 and 2.5 for both labs. We note that all the I_c measurements are either well or very well characterised, consistent with the technical requirement for excellent data, accurate to better than a few percent, and the large cost and manpower they incur.

iii) Poorly characterised random lab errors [IT(n-value, RRR, Q, CnC and Plating thickness), BR(RRR) and Nb–Ti(n-value, RRR, Q, CnC, Strand diameter and Plating thickness)]: These twelve measurement types have a range of lab errors in at least one of the labs that is smaller than 0.25. One third of these measurements have a ratio

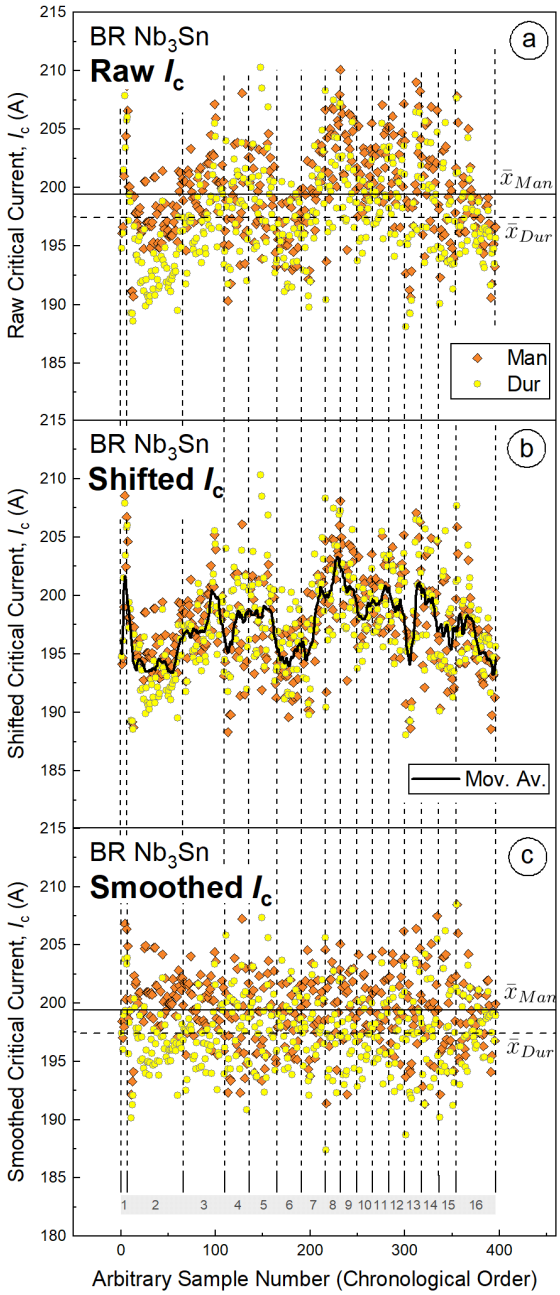

Figure 10: The Durham (Dur) and manufacturer (Man) I_c data for the bronze route (BR Nb_3Sn) strands in chronological order. ⓐ Raw data, ⓑ a 20-point moving average (MA) of the Durham data and the manufacturer data after the latter has been shifted to the Durham mean and ⓒ the raw data from both labs after subtracting the MA and the mean of the manufacturer data has been restored. The strands received by Durham were grouped into 17 individual deliverables represented here by vertical dashed lines.

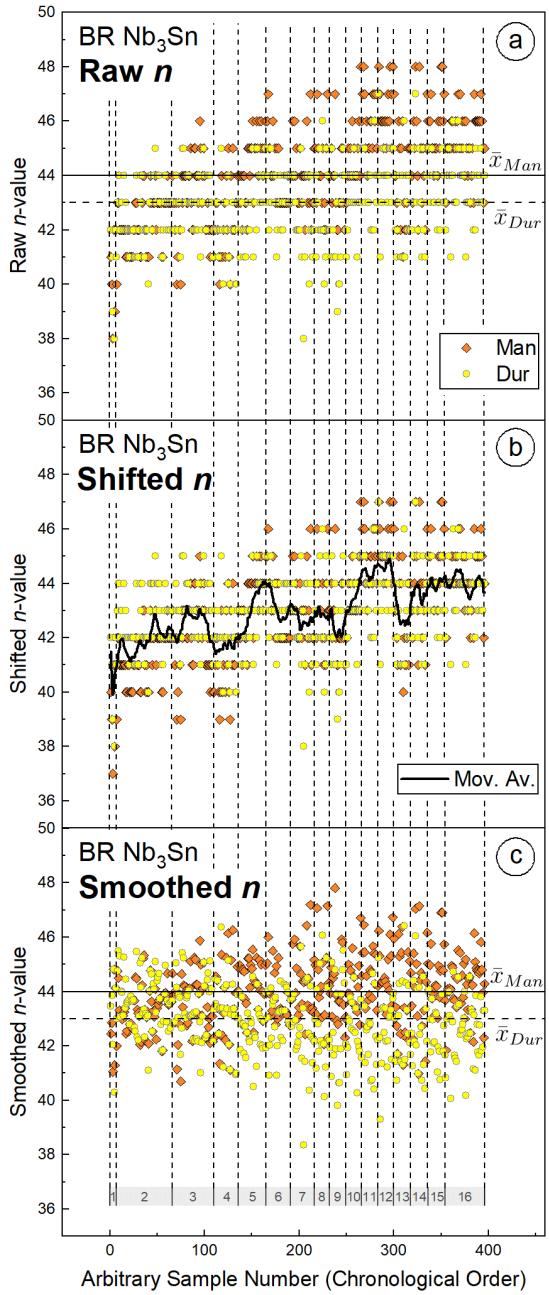

Figure 11: The Durham (Dur) and manufacturer (Man) n-value data for the bronze route (BR Nb_3Sn) strands in chronological order. ⓐ Raw data, ⓑ a 20-point moving average (MA) of the Durham data and the manufacturer data, after the latter has been shifted to the Durham mean and ⓒ the raw data from both labs after subtracting the MA and the mean of the manufacturer data has been restored. The strands received by Durham were grouped into 17 individual deliverables represented here by vertical dashed lines.

greater than 10. The n-value, Q, CnC and plating thickness measurements for both the internal tin and Nb–Ti strands, and the RRR measurements for all three strands have high ratios.

When the range of the random lab error is large, the data include a large range for the possible differences between adjacent strands. If we were confident that the estimated lab errors included all the important sources of error (i.e. the standard single lab assumption), we could take the minimum values for the random lab errors and the maximum values for the variability of the strands. Alternatively, were the properties of the adjacent strands essentially identical and the variability between adjacent strand properties much smaller than the variability between piece-length end properties, it would mean there were significant errors not identified in the estimates and we could take the complementary values - the maximum values for the lab estimates and the minimum values for the variability of the strands. In general, we would expect values between these two limits, and for example, interpret the large IT(RRR) lab maximum values of 16.4 % and 19.0 % for Durham and the manufacturer respectively as follows: it is unlikely that the IT(RRR) lab errors are close to these large values, given the BR(RRR) data are more than a factor 6 smaller and that RRR values are determined by the copper matrix and not the superconductor. Hence, we suggest the associated assumption, that it is unlikely that the adjacent strands are identical (perfectly correlated). If we assume that the lab errors in Durham were smaller, so say $\tilde{\sigma}_{Dur,\,Dtd,\,Smd} = 7\,\%$ and the value of $\tilde{\sigma}_{Lab,\,Smd}$ unchanged, the measured value of $\tilde{\sigma}_{\Delta,\,Adj}$ would be smaller. The equivalent set of values would then be $\tilde{\sigma}_{\Delta,\,Adj} = 13.9\,\%$, $\tilde{\sigma}_{Man,\,Dtd,\,Smd} = 12.0\,\%$ and $\tilde{\sigma}_{P.Lth,\,Smd} = 17.1\,\%$. This demonstrates the general result for interpreting measurements with a large range of lab error: if better measurements reduced one of the lab errors to be closer to its minimum value, the equivalent value for the other lab would also be closer to its minimum value and the piece-length value closer to its maximum value.

iv) Single lab errors [BR(Plating thickness) and BR(Twist pitch)]: For our single lab measurements (where we have no complementary manufacturer measurements), it is not possible to calculate a range for the lab error. Here, we have used destructive methods to characterise the plating thickness and twist pitch, although future work could include non-destructive repeat measurements to better measure the lab errors. For the BR(Plating thickness) measurements, the estimated lab error is very small (0.2 %) compared to the raw data (14.7 %). Without measurements from a second lab, one can only really make the standard single lab assumption that the estimated lab errors are accurate, and conclude that the large variance of the raw measurements is almost entirely due to the variance of the strand properties. The BR(Twist pitch) measurement is a special case for a single lab measurement, because the width of the raw data (6 %) is similar to the estimated lab errors (8 %). We then set $\tilde{\sigma}_{Dur,\,Dtd,\,Raw}$ to 6 % and consistent with Eq. 6 set $\tilde{\sigma}_{P.Lth,\,Raw}$ to 0 %. This demonstrates that a consequence of this particular single lab well characterised measurement is that the variability of the strands is small.

9.2 The range of the variability of the strands.

Just as we considered the range of lab errors, we can also consider the range of the variability of the strands using the ratio of the maximum random strand variability to its minimum (i.e. $\tilde{\sigma}_{P.\,Lth,\,Smd\,or\,Raw}(\mathrm{Max})/\tilde{\sigma}_{P.\,Lth,\,Smd\,or\,Raw}(\mathrm{Min})$). This ratio establishes how well the variability of the strands is characterised. There are just three measurements where the range of the strand variability is larger than 2.5 [IT(Q) and Nb–Ti(CnC and Strand diameter)] and in all three cases the properties of the strands are well within the ITER specification requirements (cf. Ratio 3 below). We conclude that the variability of the strands is generally very well characterised in this work.

9.3 The correlation between the adjacent strand data.

The correlation of the adjacent strand data from the two labs can be characterised by the ratio of the NSD of the difference between the measurements on adjacent strands ($\tilde{\sigma}_{\Delta,\,Adj}$) to the equivalent random value, were pairs of strands randomly chosen ($\tilde{\sigma}_{\Delta,\,Rand,\,Smd\,or\,Raw}$). There are five measurements where adjacent strand data from the two laboratories are weakly correlated as evidenced by the values of $\tilde{\sigma}_{\Delta,\,Adj}$ being just a little less than $\tilde{\sigma}_{\Delta\,Rand,\,Raw}$: IT($Q$ and Twist Pitch) and Nb–Ti(n-value, strand diameter and twist pitch). Despite the ratio being close to unity and containing relatively little information [49], it is useful. For example, the IT(Twist pitch) data analysis attributes most of the width in the distribution of the raw data (i.e. 5.2 % and 5.9 %) to the random errors from the labs (i.e. 4.9 % and 5.7 %) rather than the variability of the strands (i.e. 1.7 %). Analysis of the IT(Q and Twist pitch) and Nb–Ti(n-value) measurements using the 20 point smoothing produces non-physical (negative) oversmoothed values with negative variances and adjacent strand data becoming anti-correlated as discussed with Figure 6. As can be seen in Tables 5 - 7, the maximum lab errors from the raw data (i.e. $\tilde{\sigma}_{Lab,\,Dtd,\,Raw}(\mathrm{Max})$) are similar to their equivalent raw data (i.e. $\tilde{\sigma}_{Lab,\,Raw}$), and the minimum raw values for the piece-lengths are small, consistent with Eqs 17 to 19, rewritten in terms of Bienayme's identity. When $\tilde{\sigma}_{\Delta,\,Adj}$ is very similar to $\tilde{\sigma}_{\Delta\,Rand,\,Raw}$, the small amount of information from the correlation between the adjacent strands can be either extracted as the moving average or as the random error depending on the window size (cf. Table 4). For the Nb–Ti(Strand diameter and twist pitch) where smoothing does produce physical results, the small amount of additional information in $\tilde{\sigma}_{\Delta,\,Adj}$ means as expected, that the maximum lab errors from the smoothed data (i.e. $\tilde{\sigma}_{Lab,\,Dtd,\,Smd}(\mathrm{Max})$) are similar to raw data values (i.e. $\tilde{\sigma}_{Lab,\,Dtd,\,Raw}(\mathrm{Max})$).

Clearly the most interesting cases arise when $\tilde{\sigma}_{\Delta,\,Adj}$ is much less than $\tilde{\sigma}_{\Delta\,Random}$. The four lowest ratio values occur for the BR Nb_3Sn. In these cases, the lab errors and the variability of the adjacent strand properties are both much smaller than the variability of the piece-length ends, and the strong correlation between adjacent strand data brings significant new information that drives the maximum lab error much closer to its minimum value. For example, for the BR Nb_3Sn losses measurements where $\tilde{\sigma}_{\Delta,\,Adj} = 0.32$, although the width of the smoothed data from Durham is 13.8 %, it

is deconvoluted (as shown in Table 6) into a maximum of only $\sim 4.3\,\%$ that comes from the lab errors and a large minimum value of $\sim 13.1\,\%$ for the strand variability - separating the lab errors and strand variability in this way demonstrates how two lab processing-and-measuring on adjacent strands, can be a proxy for single lab repeat measurements.

10 Figures of merit

Here, we consider three ratios that are figures of merit, where large values are preferred. They are used to inform our discussion and recommendations.

10.1 Unidentified random lab errors.

The first ratio given in the top 3 rows of Table 8 is the ratio of the estimated random error to the minimum random lab error (i.e. $\tilde{\sigma}_{Est,\,Rand}/\tilde{\sigma}_{Lab,\,Dtd,\,Smd\,or\,Raw}(\mathrm{Min})$) It identifies those measurements where there are significant sources of lab error that have not been identified in the Durham lab random error estimates and is highlighted and underlined when less than 0.4.

Consider first the Nb–Ti(RRR) measurements where the range for the lab error in Durham ($\tilde{\sigma}_{Dur,\,Dtd,\,Smd}$) is from 4.0 to 6.8 %. This includes a minimum value that is four times larger than the estimated random error in Durham of 1 % (which gives a ratio of 0.25 in Table 8). Similarly, the IT(RRR) range for $\tilde{\sigma}_{Man,\,Dtd,\,Smd}$ of 9.9 to 19 % also includes a minimum value that is five times larger the estimated error from Durham. We conclude that there simply must be additional random errors in the processing/measurements that are not included in Durham's estimated errors. The conclusion about these data is robust - it holds whether we consider raw data or smoothed data, and whether the adjacent strand properties are correlated or not.

Similar, reasoning suggests that the manufacturer's measured lab errors also have unidentified sources of error associated with the IT(n-value, Q, and Plating thickness), BR(Q) and Nb–Ti(n-value) measurements as shown in Table 8. In these cases, although Durham minimum values are equal to the estimated values, because they are lower bounds, it doesn't rule out that there are unidentified errors in both labs. Equally, the Durham lab should investigate the Nb–Ti(CnC ratio and Plating thickness) to find unidentified sources of errors.

10.2 Unidentified systematic errors.

The second ratio given in the middle 3 rows of Table 8 is the estimated systematic error divided by the difference in the averages from the two labs (i.e. $\tilde{\sigma}_{Est,\,Syst}/\Delta\bar{x}$). It identifies whether the difference in the average of the measurements from Durham and the manufacturer is significantly different to the estimated systematic error from Durham (Negative values imply that the manufacturers' values are higher than Durham's). For example, the Durham Nb–Ti n-value data have a systematic error

estimated to be 1 %, although the difference between the average n-values for Durham and the manufacturer is 13 %. We conclude that there simply must be large systematic errors in the n-values either in Durham or for the manufacturer that are not included in the Durham estimates. Table 8 shows that there are 12 measurements (in bold and underlined) that have the ratio lower than 0.25, associated with measurements that have unidentified or poorly characterised systematic lab errors. We note that for verification measurements where as-supplied strands are destructively processed and measured, practical standard materials with a reproducibility of even as high as 1 %, or exchange of strands (for measurement alone) and personnel would be useful to eliminate systematic errors.

10.3 Strands routinely meeting ITER specifications

The bottom 3 rows of Table 8 give a ratio that provides a measure of how likely the strands are to meet the ITER specifications (i.e. $(100 \times (\bar{x}_{Lab,\,Smd\,or\,Raw} - x_{ITER}))/(3\tilde{\sigma}_{P.Lth,Min\,tot} \times \bar{x}_{Dur})$). It is given in terms of the definition of the normalised minimum total strand variance ($\tilde{\sigma}^2_{P.Lth,Min\,tot}$) where,

$$\tilde{\sigma}^2_{P.Lth,Min\,tot} = \tilde{\sigma}^2_{P.Lth,\,Smd\,or\,Raw}(Min) + \tilde{\sigma}^2_{MA}\,. \tag{27}$$

and makes the ratio similar to the process capability index [50]. For the BR(RRR) strands, the normalised minimum total strand variance (i.e. 9.6 %), which includes contributions in quadrature from both the random average (i.e. 6.5 %) and the moving average (i.e. 7.1 %), when divided by the difference between the ITER specification and the Durham average gives a ratio of 1.6 as shown in Table 8. The equivalent value for the manufacturer of 0.7 is a lower bound, and therefore not inconsistent with the high value of 1.6 found in Durham. This last ratio has an immediate impact on verification measurements. If it is large, the strands are comfortably above the ITER specification and there is less commercial interest in whether the measurement is accurate or well characterised or not. If it is small (only values less than or equal to 0.5 are in bold and underlined in Table 8), a significant fraction of the strands will not meet the ITER specification. As shown in the bottom three rows of Table 8, only the RRR measurements on Nb_3Sn bring this concern.

Table 8: Figures of merit: Large numbers represent desirable properties. Small numbers (in bold and underlined) represent undesirable properties. Top 3 data rows: Ratio of the estimated random error to the minimum random lab error (i.e. $\tilde{\sigma}_{Est,\,Rand}/\tilde{\sigma}_{Lab,\,Dtd,\,Smd\,or\,Raw}$(Min)). Middle 3 data rows: Ratio of the estimated systematic error to the difference in the averages (i.e. $\tilde{\sigma}_{Est,\,Syst}/\Delta\bar{x}$) from the two labs. Bottom 3 rows of data: The difference between the ITER specification and the Durham mean divided by three times the minimum total strand variability (i.e. $(100 \times (\bar{x}_{Lab,\,Smd\,or\,Raw} - x_{ITER}))/(3\tilde{\sigma}_{P.Lth,Min\,tot} \times \bar{x}_{Dur})$) where x_{ITER} is the ITER specification taken from Table 2). The abbreviations used are I_c: critical current; n-value: index of transition; RRR: residual resistivity ratio; Q: hysteretic losses; CnC ratio: copper to non-copper ratio.

Ratio	Strand type	I_c		n-value		RRR		Q		CnC ratio		Strand diameter		Twist pitch		Plating thickness	
		Dur	Man	Dur	Man	Dur	Man	Dur	Man	Dur	Man	Dur	Man	Dur	Man	Dur	Man
Estimated random error to minimum random lab error	IT	1.0	0.71	1.0	**0.18**	1.0	**0.20**	1.0	**0.17**	0.43	1.0	1.1	1.3	1.6	1.4	2.0	**0.03**
	BR	1.7	1.9	1.0	1.1	1.0	1.3	1.0	**0.25**	1.0	0.71	1.4	2.0	n/a	n/a	n/a	n/a
	Nb-Ti	1.0	1.3	1.0	**0.19**	**0.25**	1.0	1.0	0.42	**0.08**	1.0	0.71	1.0	1.5	2.0	**0.05**	1.0
Estimated systematic error to difference in the averages from two labs	IT	-0.62		**-0.18**		**-0.09**		**0.24**		0.67		0.56		**-0.10**		**-0.02**	
	BR	-1.5		-0.72		**-0.12**		**-0.17**		-1.9		-14		n/a		n/a	
	Nb-Ti	**0.20**		**-0.07**		**-0.33**		0.55		**-0.05**		7.3		1.7		**-0.10**	
Difference between the lab mean value and the ITER specification to three times the minimum total strand variation	IT	2.1	2.2	1.6	1.9	**0.4**	**0.5**	-7.2	-7.9	1.0	0.8	2.9	2.4	1.8	3.7	0.6	0.9
	BR	0.7	0.9	6.7	7.0	**0.2**	**0.5**	-11.4	-11.2	0.6	0.7	2.0	2.0	n/a	n/a	n/a	n/a
	Nb-Ti	1.8	1.3	7.6	8.7	0.9	1.0	-2.6	-3.1	0.6	1.0	5.0	4.9	3.1	3.0	1.5	1.70

11 Discussion and recommendations

Finally, we discuss the measurements in turn and make recommendations. We focus on the low ratios in Table 8 that highlight measurements (first and second ratio) and strand properties (third ratio), that need work.

Among the I_c measurements, only the systematic differences between the two labs (second ratio) for Nb–Ti are small. Given that there is no processing for Nb–Ti, we suggest these differences originate with calibration of instruments or systematic errors in analysis. For this and all the five measurements on Nb–Ti that have this ratio small, we recommend exchange of strands (as per the RRR and loss measurements here), exchange of equipment such as standard resistors, and importantly, exchange of staff.

Identifying the source of inaccurate n-value measurements is difficult remotely because of the complexity of the measurements: n-values can be artificially increased if the strand is grossly damaged or gas generated by resistive heating in the probes stays in the magnet bore and insulates the strands so they heat during the $E - J$ transition, if the strand moves and there is premature quenching, or if the high purity copper in the strands has been polluted by tin. Equally, n-values can be artificially decreased if the strand is marginally damaged and there is large-scale inter-filament current flow, or if the time-constants of the instruments used are not sufficiently short. Since n-values are not thermodynamic properties, they are also sensitive to the ramp rates of the current during the measurement and the history of the magnetic field. In this work, if the effects of barrier rupture during the heat-treatment are important, they will contribute to both the systematic and random lab errors since the two labs heat-treat the strands independently. Given the need for HTS straps to improve the n-values (Section 4.2) and the low first and second ratios for IT Nb_3Sn strands, we propose focusing on reducing the mechanical damage during processing-and-measurement. We recommend better ensuring the strands do not stick to the barrels during the heat-treatment and developing single-part standardised barrels. Such robust barrels would also enable round-robin (transport and) measurements between different labs using clamped electrical connections to pre-existing voltage taps and current leads, without the need for participant labs to apply any heat to the strands.

We found large systematic changes in RRR with gas purity for IT Nb_3Sn (Section 5.2), as well as a large number of small ratios in Table 8 for both IT and BR Nb_3Sn. We recommend standardising and monitoring the purity of the gas during the heat-treatment for Nb_3Sn strands (e.g. to manage outgasing). Alternatively, a cheaper option would be to react copper wires (or perhaps some copper extracted from the strands) together with the strands themselves and check them after reaction to verify the gas purity. Less important, thermocouple thermometry is cheap, mechanically robust and has well-established excellent thermal cycling reproducibility. Nevertheless, we found significant outliers and variations in voltage-temperature calibrations of commercial thermocouples. It would be beneficial to use thermocouples with tighter calibration tolerances, or better still, replace the thermocouple thermometry with calibrated

resistance thermometry and use furnaces with better homogeneity.

The first two figures of merit ratios are low for the losses measurements (Q) of both BR and IT Nb_3Sn strands. This is in contrast to the markedly larger values for the Nb–Ti and suggests that either the brittle nature of Nb_3Sn or the heat-treatment is the primary origin of the random and systematic errors in Q. Losses in multifilamentary Nb_3Sn have a contribution from the filaments themselves but bridges between them and the coalescing of filaments very significantly increases losses [51]. Hence, we attribute the high ratios to these bridges being much more sensitive to processing, barrier rupture and/or handling than the filaments themselves, and hence Q having many more low values for these ratios than I_c. We recommend the use of a barrier to prevent the strands from sticking to the Ti-alloy during the heat-treatment (as above for n-value), standardised cutting of the strands to length, and better mechanical support for the (tightly coiled) strands during the in-field magnetic measurements to increase/improve values of the first ratio. The exchange of standard strands (e.g. Pd with the same coiled geometry) will increase values of the second ratio.

Relatively few strands did not meet the ITER specification (i.e. have low values for the third ratio) for the room temperature measurements. Although the strand diameter measurements are well characterised (i.e. the sources of random and systematic errors are known), the copper-non-copper ratio, twist pitch and plating thickness data all show some very large unidentified sources of both systematic and random error. For example: the minimum random lab error in Durham's Nb–Ti (Plating thickness) data is 18 times larger (first ratio) than the estimated random errors; the difference between the average IT Nb_3Sn (Twist pitch) data from the two labs is 9.8 times larger (second ratio) than Durham's estimated systematic error. Understandably, the commercial interest in the sources of these errors is low because there are no low numbers for the third ratio, and identifying them efficiently would require access for both sets of scientists to both labs, to further exchange know-how, analysis and data collection.

Turning now to improving the uniformity of strand manufacture (i.e. increasing the values of the third ratio): the RRR variability in the Nb_3Sn strands most probably has its origin in gas purity during the heat-treatment, but Ta diffusion barrier rupture in the IT strands is another candidate explanation as a source of random and systematic errors in the RRR values - an SEM investigation of barriers post-heat-treatment would be instructive. Table 8 shows several intermediate (≈ 0.5) values of the third ratio, where understanding the cross-correlation between the different types of measurements may help achieve better strand uniformity. Figure 12 shows some of the complexity of the information available: Figure 12 ⓐ shows that as the CnC ratio increases, I_c decreases, whereas Figure 12 ⓑ shows there is no correlation between the CnC ratio and the losses. We will need to consider how the manufacturing variability that changes the CnC ratio, simultaneously affects current density in the filaments, bridging between filaments, and say the uniformity of the filament cross-sectional areas, to explain why CnC is correlated with I_c but not with Q. Such considerations are best addressed by the manufacturers using their commercially sensitive know-how and some additional

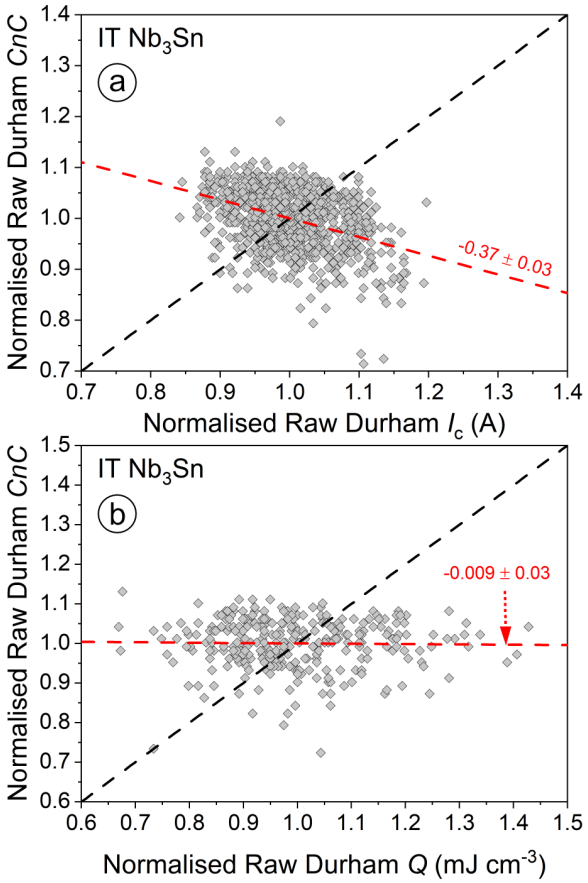

Figure 12: Cross-measurement correlations between different measurements in Durham on the internal tin (IT Nb_3Sn) strands. ⓐ Normalised copper-non-copper ratio versus normalised critical current. ⓑ Normalised copper-non-copper ratio versus normalised hysteresis losses. In both figures, the gradient for the best fit and for + 1 are shown.

analysis and measurements.

12 Final comments

It is standard commercial practice for strand manufacturers to measure the piece-length ends of strands to keep a timely oversight of any potential manufacturing problems. For those strand properties that are demanding to achieve, a fraction of the measurements will be below specification and the manufacturer has to determine to what degree it is due to strand variability (and the piece-length rejected) or lab error (and remeasure another part of the piece-length end). Equally the customer will choose to make verification measurements dependent on the cost of those measurements and the consequences of a small fraction of strands slipping through the net below specification. Some of our original motivation to engage with these large quantity verification measurements was to ensure as best as possible that only those strands that met the necessary ITER technical specifications were included in the fusion magnet

confinement systems, to help produce some of the trained fusion scientists required - the UK alone needs more than 3000 new research-trained fusioneers in the next 10 years [52], and to improve verification measurements for high-field superconductors.

It has long been known that a single lab measuring strands (together with repeat measurements) or round-robin measurements can separately identify strand variability and lab errors. In this paper, where there are no standards materials for the processing-and-measurements required and the processing is irreversible (with similarities to destructive measurements), we have shown that two independent labs measuring adjacent strands can serve as a proxy for two lab round-robin measurements and hence identify drift, upper and lower bounds for the random and systematic lab errors, as well as the variability of the strands. This has enabled us to identify more than a dozen measurements (cf. Table 8) where there are significant unidentified lab errors and conclude that improvements in the heat-treatment processing, and development of practical standard materials, that can be processed and measured reproducibly, even to say just 1 % (particularly for those measurements with low ratios in Table 8), would be valuable.

Acknowledgments

The data are available at: https://dx.doi.org/.... and associated materials are on the Durham Research Online website: http://dro.dur.ac.uk/. We would like to thank everyone who has helped make this project the success it has been. Special and particular thanks are given to Andrea Dawson, Craig Robinson, Matthew Plumb, Emily Roe and Mike McBreen. We also thank David Pattinson for his help with the microscopy and Steve Lishman (and his team) for all the work completed in the Durham Mechanical Workshop. We would like to thank David Cardwell and colleagues at Cambridge, Arend Nijhuis and his colleagues at Twente, as well as colleagues at CERN and NIST for the cross-checking data.

References

[1] M. J. Raine, S. A. Keys, and D. P. Hampshire, "Characterisation of the transport critical current density for conductor applications," in *Handbook of Superconductivity*. CRC Press, 2022, pp. 177–208.

[2] B. S. Lim, F. Simon, Y. Ilin, C. Y. Gung, C. Boyer, C. Beemsterboer, P. Valente, S. Lelekhov, and N. Mitchell, "Development of the ITER PF coils," *IEEE Transactions on Applied Superconductivity*, vol. 22, no. 3, p. 4, 2012.

[3] K. Dulon, "Toroidal field coils: strand production passes 400 tonnes," 2013. [Online]. Available: https://www.iter.org/newsline/276/1653

[4] A. Vostner, M. Jewell, I. Pong, N. Sullivan, A. Devred, D. Bessette, G. Bevillard, N. Mitchell, G. Romano, and C. Zhou, "Statistical analysis of the Nb_3Sn strand production for the ITER toroidal field coils," *Superconductor Science & Technology*, vol. 30, no. 4, p. 14, 2017.

[5] M. Sborchia, E. Barbero Soto, R. Batista, B. Bellesia, A. Bonito Oliva, E. Boter Rebollo, T. Boutboul, B. E, J. Caballero, M. Comelis, J. Fanthome, R. Harrison, M. Losasso, A. Portone, H. Rajainmaki, P. Readman, and P. Valente, "Overview of ITER magnet system and European contribution," *IEEE/NPSS 24^{th} Symposium on Fusion Engineering*, pp. 1–8, 2011.

[6] I. Pong, M. C. Jewell, B. Bordini, L. R. Oberli, S. Liu, F. Long, T. Boutboul, P. Readman, S. H. Park, P. Y. Park, V. Pantsyrny, V. Tronza, N. Martovetsky, J. Lu, and A. Devred, "Worldwide benchmarking of ITER internal tin Nb_3Sn and NbTi strands test facilities," *IEEE Transactions on Applied Superconductivity*, vol. 22, no. 6, p. 1, 2012.

[7] M. C. Jewell, T. Boutboul, L. R. Oberli, F. Liu, Y. Wu, A. Vostner, T. Isono, Y. Takahashi, S. H. Park, A. Shikov, A. Vorobieva, N. Martovetsky, K. Seo, D. Bessette, and A. Devred, "World-wide benchmarking of ITER Nb_3Sn strand test facilities," *IEEE Transactions on Applied Superconductivity*, vol. 20, no. 3, pp. 1500–1503, 2010.

[8] "CERN to be reference lab for ITER's superconductor tests," 2010, https://cerncourier.com/cern-to-be-reference-lab-for-iters-superconductor-tests/ [Accessed: 08/08/2024].

[9] "Durham superconductivity group," 2019, http://community.dur.ac.uk/superconductivity.durham/ [Accessed: 08/08/2024].

[10] D. R. McGuire, J. Lu, S. Hill, K. Dellinger, T. Sloan, K. Chan, and N. N. Martovetsky, "Verification testing of ITER Nb_3Sn strand at the NHMFL," *IEEE Transactions on Applied Superconductivity*, vol. 25, no. 3, pp. 1–4, 2015.

[11] F. Liu, H. J. Liu, B. Liu, F. Long, L. Qian, and C. Chen, "ITER Nb_3Sn and NbTi strands benchmarking at ASIPP," *IEEE Transactions on Applied Superconductivity*, vol. 24, no. 3, p. 4, 2014.

[12] F. Liu, H. Liu, S. Liu, B. Liu, L. Lei, and Y. Wu, "NbTi strands verification for ITER PF CICC process qualification of CNDA," *Journal of Physics: Conference Series*, vol. 507, 2014.

[13] "Japan Atomic Energy agency," 2019, https://www.jaea.go.jp/english/ [Accessed: 08/08/2024].

[14] "KFE Korea Institute of Fusion Energy," 2022, https://www.kfe.re.kr/eng [Accessed: 08/08/2024].

[15] Y. Karasev, A. Malchenkov, P. Lukyanov, M. Polikarpova, V. Pantsyrny, I. Abdyukhanov, Y. Konovalov, L. Potanina, S. Lelechov, T. Baumgartner, M. Eisterer, and H. W. Weber, "Characterization of Nb-Ti strands in the process of industrial production for the ITER poloidal field coils," *IEEE Transactions on Applied Superconductivity*, vol. 26, no. 4, 2016.

[16] Y. V. Karasev, V. I. Pantsyrny, M. V. Polikarpova, P. A. Lukianov, L. V. Potanina, T. Baumgartner, M. Eisterer, and H. W. Weber, "$J_c(B,T)$ characterization of commercial NbTi strands for the ITER poloidal field coils by transport and magnetization methods," *IEEE Trans. Appl. Supercond.*, vol. 23, no. 3, 2013.

[17] T. Boutboul, V. Abaecherli, G. Berger, D. Hampshire, J. Parrell, M. Raine, P. Readman, B. Sailer, K. Schlenga, M. Thoener *et al.*, "European Nb_3Sn superconducting strand production and characterization for ITER TF coil conductor," *IEEE Transactions on Applied Superconductivity*, vol. 26, no. 4, pp. 1–4, 2016.

[18] C. Zhou, Y. Miyoshi, E. P. A. v. Lanen, M. Dhallé, and A. Nijhuis, "Direct measurement of inter-filament resistance in various multi-filamentary superconducting NbTi and Nb_3Sn strands," *Superconductor Science and Technology*, vol. 25, no. 1, p. 015013, 2012.

[19] "Annex B: Technical specification for strand characterization of TF Nb_3Sn samples," ITER specification document, 2010.

[20] "Kanthal furnace tubes," https://www.kanthal.com/en/products/furnace-products/furnace-tubes/ [Accessed: 08/08/2024].

[21] "Super clean (base-plate design) kit," https://www.sigmaaldrich.com/GB/en/product/supelco/28878u [Accessed: 08/08/2024].

[22] A. Dobi, D. S. Leonard, C. Hall, L. J. Kaufman, T. Langford, S. Slutsky, and Y. R. Yen, "Study of a zirconium getter for purification of xenon gas," *Nuclear Instruments and Methods in Physics Research Section A: Accelerators, Spectrometers, Detectors and Associated Equipment*, vol. 620, no. 2–3, pp. 594–598, 2010.

[23] H. Müller and T. Schneider, "Heat treatment of Nb_3Sn conductors," *Cryogenics*, vol. 48, pp. 323–330, 2008.

[24] N. Cheggour, T. C. Stauffer, W. Starch, P. J. Lee, J. D. Splett, L. F. Goodrich, and A. K. Ghosh, "Precipitous change of the irreversible strain limit with heat-

treatment temperature in Nb_3Sn wires made by the restacked-rod process," *Scientific Reports*, vol. 8, p. 8, 2018.

[25] J. Lu, D. R. McGuire, S. Hill, R. Niu, K. Chan, and N. N. Martovetsky, "Influence of heat treatment excursion on critical current and residual resistivity ratio of ITER Nb_3Sn strands," *Superconductor Science Technology*, vol. 30, no. 7, p. 8, 2017.

[26] J. Ekin, N. Cheggour, L. Goodrich, J. Splett, B. Bordini, D. Richter, and L. Bottura, "Extrapolative scaling expression: A fitting equation for extrapolating full $I_c(B, T, \epsilon)$ data matrices from limited data," *IEEE Transactions on Applied Superconductivity*, vol. 27, no. 4, pp. 1–7, 2017.

[27] F. Fickett, "Oxygen annealing of copper: A review," *Materials Science and Engineering*, vol. 14, no. 3, pp. 199–210, 1974. [Online]. Available: https://www.sciencedirect.com/science/article/pii/0025541674901001

[28] M. J. Raine, S. A. Keys, and D. P. Hampshire, *Handbook of Superconducting Materials*, 2nd ed. Taylor & Francis, 2017, ch. Characterisation of the Transport Critical Current Density for Conductor Applications.

[29] J. W. Ekin, *Experimental Techniques for Low-Temperature Measurements*. New York: Oxford University Press, 2007.

[30] "Department of geography weather," https://weather.awh.durham.ac.uk/weather/current_vantage.htm [Accessed: 08/08/2024].

[31] W. J. Nuttall, R. H. Clarke, and B. A. Glowacki, "Stop squandering helium," *Nature*, vol. 485, p. 573, 2012.

[32] P. Sunwong, J. S. Higgins, and D. P. Hampshire, "Probes for investigating the effect of magnetic field, field orientation, temperature and strain on the critical current density of anisotropic high-temperature superconducting tapes in a split-pair 15 T horizontal magnet," *Review of Scientific Instruments*, vol. 85, no. 6, p. 065111, 2014.

[33] L. F. Goodrich, L. T. Medina, and T. C. Stauffer, "Repeatability of critical-current measurements on Nb_3Sn and Nb-Ti wires," *IEEE Transactions on Applied Superconductivity*, vol. 7, no. 2, pp. 1508–1511, 1997.

[34] "F4E-OMF-405 Technical Specification (Annex B): Technical Specification for the Strand Characterisation of PF NbTi Samples," ITER specification document, 2012.

[35] D. M. J. Taylor and D. P. Hampshire, "Relationship between the n-value and critical current in Nb_3Sn superconducting wires exhibiting intrinsic and extrinsic behaviour," *Superconductor Science and Technology*, vol. 18, no. 12, p. S297, nov 2005. [Online]. Available: https://dx.doi.org/10.1088/0953-2048/18/12/012

[36] M. C. Jewell, "The effect of strand architecture on the fracture propensity on niobium-tin composite wires," Thesis, 2008. [Online]. Available: http://search.proquest.com/docview/304449590?accountid=14533

[37] "Gold plated brass annealing trials and annealed C101 copper residual resistivity

ratio," https://www.cv.nrao.edu/~akerr/Annealing.pdf [Accessed: 08/08/2024]. [Online]. Available: https://www.cv.nrao.edu/~akerr/Annealing.pdf

[38] N. Cheggour, P. J. Lee, L. F. Goodrich, Z. H. Sung, T. C. Stauffer, J. D. Splett, and M. C. Jewell, "Influence of the heat-treatment conditions, microchemistry, and microstructure on the irreversible strain limit of a selection of Ti-doped internal-tin Nb_3Sn ITER wires," *Superconductor Science & Technology*, vol. 27, no. 10, p. 21, 2014.

[39] D. S. Easton and D. M. Kroeger, "Kirkendall voids - detriment to Nb_3Sn superconductors," *IEEE Transactions on Magnetics*, vol. 15, no. 1, pp. 178–181, 1979.

[40] I. Pong, S. C. Hopkins, X. Fu, B. A. Glowacki, J. A. Elliott, and A. Baldini, "Microstructure development in Nb_3Sn (Ti) internal tin superconducting wire," *Journal of Materials Science*, vol. 43, no. 10, pp. 3522–3530, 2008.

[41] C. Scheuerlein, M. Di Michiel, and A. Haibel, "On the formation of voids in internal tin Nb_3Sn superconductors," *Applied Physics Letters*, vol. 90, no. 13, p. 3, 2007.

[42] Q. Design, "Magnetometry." [Online]. Available: https://qd-uki.co.uk/wp-content/uploads/2019/07/Magnetometry-Application-Note.pdf

[43] S. Foner, "Vibrating sample magnetometer," *Review of Scientific Instruments*, vol. 27, p. 548, 1956.

[44] I. J. Daniel and D. P. Hampshire, "Harmonic calculations and measurements of the irreversibility field using a vibrating sample magnetometer," *Phys. Rev. B*, vol. 61, pp. 6982–6993, Mar 2000. [Online]. Available: https://link.aps.org/doi/10.1103/PhysRevB.61.6982

[45] "Yorkshire precision gauges," https://www.ypg-ltd.com/ [Accessed: 08/08/2024].

[46] "COULOSCOPE® CMS2 and COULOSCOPE® CMS2 step," https://www.ultraprecisao.com/storage/files/original/2018/01/BROC_COULOSCOPE_CMS2_CMS2STEP_942-008_en.pdf [Accessed: 08/08/2024].

[47] "Coefficient of variation," https://itl.nist.gov/div898/software/dataplot/refman2/auxillar/coefvari.htm [Accessed: 08/08/2024].

[48] A. Savitzky and M. J. E. Golay, "Smoothing and differentiation of data by simplified least squares procedures," *Anal. Chem.*, vol. 36, pp. 1627–1639, 1964.

[49] "Information theory for continuous systems," https://www.library.uc.edu.kh/userfiles/pdf/11.Information%20Theory%20For%20Continuous%20Systems..pdf [Accessed: 08/08/2024].

[50] V. Tiwari and N. Singh, "Review in the development in process capability analysis," *International Journal of Scientific and engineering research*, vol. 4, no. 7, pp. 2471–2475, 2013.

[51] R. Goldfarb and J. Ekin, "Hysteresis losses in fine filament internal-tin superconductors," *Cryogenics*, vol. 26, no. 8, pp. 478–481, 1986.

[52] "UK Fusion Materials Roadmap 2025," UKAEA, to be published.